Inorganic Chemistry

pubs.acs.org/IC

Featured Article

A Mononuclear and High-Spin Tetrahedral Ti^{II} Complex

Anders Reinholdt, Daniel Pividori, Alexander L. Laughlin, Ida M. DiMucci, Samantha N. MacMillan, Mehrafshan G. Jafari, Michael R. Gau, Patrick J. Carroll, J. Krzystek, Andrew Ozarowski, Joshua Telser,* Kyle M. Lancaster,* Karsten Meyer,* and Daniel J. Mindiola*

Cite This: *Inorg. Chem.* 2020, 59, 17834–17850

Read Online

ACCESS | Metrics & More | Article Recommendations | Supporting Information

ABSTRACT: A high-spin, mononuclear Ti^{II} complex, $[(Tp^{tBu,Me})TiCl]$ [$Tp^{tBu,Me-}$ = hydridotris(3-*tert*-butyl-5-methylpyrazol-1-yl)borate], confined to a tetrahedral ligand-field environment, has been prepared by reduction of the precursor $[(Tp^{tBu,Me})TiCl_2]$ with KC_8. Complex $[(Tp^{tBu,Me})TiCl]$ has a $^3A_2$ ground state (assuming C_{3v} symmetry based on structural studies), established *via* a combination of high-frequency and -field electron paramagnetic resonance (HFEPR) spectroscopy, solution and solid-state magnetic studies, Ti K-edge X-ray absorption spectroscopy (XAS), and both density functional theory and ab initio (complete-active-space self-consistent-field, CASSCF) calculations. The formally and physically defined Ti^{II} complex readily binds tetrahydrofuran (THF) to form the paramagnetic adduct $[(Tp^{tBu,Me})TiCl(THF)]$, which is impervious to N_2 binding. However, in the absence of THF, the Ti^{II} complex captures N_2 to produce the diamagnetic complex $[(Tp^{tBu,Me})TiCl]_2(\eta^1,\eta^1;\mu_2\text{-}N_2)$, with a linear Ti═N═N═Ti topology, established by single-crystal X-ray diffraction. The N_2 complex was characterized using XAS as well as IR and Raman spectroscopies, thus establishing this complex to possess two Ti^{III} centers covalently bridged by an N_2^{2-} unit. A π acid such as CNAd (Ad = 1-adamantyl) coordinates to $[(Tp^{tBu,Me})TiCl]$ without inducing spin pairing of the d electrons, thereby forming a unique high-spin and five-coordinate Ti^{II} complex, namely, $[(Tp^{tBu,Me})TiCl(CNAd)]$. The reducing power of the coordinatively unsaturated Ti^{II}-containing $[(Tp^{tBu,Me})TiCl]$ species, quantified by electrochemistry, provides access to a family of mononuclear Ti^{IV} complexes of the type $[(Tp^{tBu,Me})Ti{=}E(Cl)]$ (with E^{2-} = $NSiMe_3$, N_2CPh_2, O, and NH) by virtue of atom- or group-transfer reactions using various small molecules such as N_3SiMe_3, N_2CPh_2, N_2O, and the bicyclic amine 2,3:5,6-dibenzo-7-azabicyclo[2.2.1]hepta-2,5-diene.

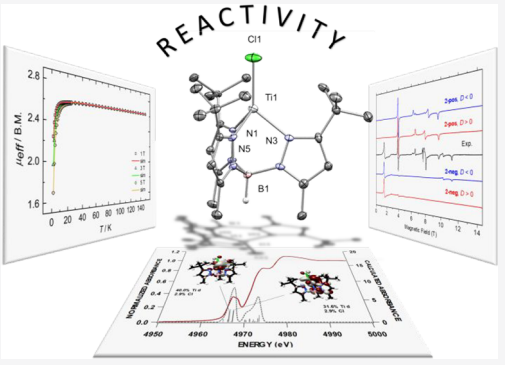

INTRODUCTION

Divalent Ti compounds have been widely used in C−C bond coupling reactions, such as the Kulinkovich or McMurry type reactions,[1] and recently in catalytic C−N bond coupling reactions by Tonks.[2] However, the coordination chemistry of isolable Ti^{II} is largely restricted to octahedral systems of the types $[TiX_2(L)]$ {X^- = Cl, CH_3, BH_4, and OPh and L = 2 dmpe [1,2-bis(dimethylphosphino)ethane];[3] X^- = Cl and L = 2 TMEDA (tetramethylethylenediamine), 4 pyridines;[4] X_2^{2-} = porphyrin,[5] L = 2 THF (tetrahydrofuran), 2 phosphine (-oxide)} and $[TiTp_2]$ [Tp^- = hydridotris(pyrazolyl)borate].[6] Other strategies to stabilize the large and highly reducing Ti^{II} ion are to coordinatively saturate it with soft or π acids, such as N_2,[7] CO,[8] isonitriles,[9] bipyridine,[10] 1,10-phenanthroline,[11] alkynes,[12] olefins,[13] cyclooctatetraene,[14] phosphines,[15] or bulky Cp^--based[16] ligands. Common to these strategies is the reliance on maximizing the coordination number, and, notably, low-coordinate Ti^{II} complexes continue to elude isolation. In particular, we found that no example of a four-coordinate, high-spin Ti^{II} d^2 complex exists. Despite the aforementioned cases all being formally categorized as Ti^{II}, the strongly π-accepting nature of one or more of the ligands means that the metal does not typically behave as a diradical or powerful π base. Perhaps only in the case of *trans*-$[TiCl_2(TMEDA)_2]$[4a,b] could one argue that the Ti^{II} ion represents a *bona fide* example of a high-spin d^2 configuration, given the more innocent nature of the chloride and chelating diamine ligands. However, this complex is highly unstable in solution, undergoing dinuclearization or disproportionation reactions.[17] More recently, Lin, Tilley, Ye, and co-workers as well as Deng and co-workers have used sterically bulky, cyclic (alkyl)(amino)carbene (cAAC) ligands to stabilize C_2-symmetric Ti[18] and Hf[19] centers of the type $[(cAAC)_2MCl_2]$, wherein a combination of π-accepting properties of the ligand and/or low symmetry electronically favors closed-shell ground states.

Received: September 5, 2020
Published: December 1, 2020

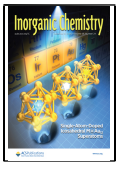

https://dx.doi.org/10.1021/acs.inorgchem.0c02586
Inorg. Chem. 2020, 59, 17834−17850

Given the propensity for mononuclear Ti^{II} to disproportionate, especially if bearing halide or pseudohalide ligands, we decided to reinvestigate its chemistry with the ubiquitous[20] Tp^- (scorpionate) ligand. Lee and co-workers established that two Tp^- ligands can be substituted onto Ti^{II}, with each being κ^3 (vide supra).[6] However, the use of more sterically encumbering groups on the pyrazoles should allow one to isolate and stabilize tetrahedral geometries with divalent ions, which has been observed for most of the 3d metals. In fact, Petrov and co-workers recently reported the synthesis of a tetrahedral divalent V^{II} complex, $[(Tp^{tBu_2})VCl]$ [Tp^{tBu_2-} = hydridotris(3,5-di(*tert*-butyl)pyrazol-1-yl)borate[21]], *via* reduction of the V^{III} precursor $[(Tp^{tBu_2})VCl_2]$.[22] Inspired by the work of Lee, Deng, Lin, Tilley, Ye, and Petrov, we have now isolated and fully characterized the only example of a high-spin, tetrahedral complex of Ti^{II}, by using a relatively weak-field ligand, in this case $Tp^{tBu,Me-}$ [$Tp^{tBu,Me-}$ = hydridotris(3-*tert*-butyl-5-methylpyrazol-1-yl)borate]. If one excludes the hypothetical compound $[Tp^RScCl]$, this Ti complex would essentially complete the divalent tetrahedral transition-metal 3d series $[Tp^RMCl]$ [Tp^{R-} = a sterically demanding κ^3-tris(pyrazolyl)borate; M = Ti, V,[22] Cr,[23] Mn,[24] Fe,[25] Co,[26] Ni,[27] Cu,[28] and Zn[29]]. Herein, we provide a reliable synthetic route to a mononuclear, high-spin Ti^{II} ion confined to a tetrahedral geometry and provide complete spectroscopic and magnetic data for this unique system, including high-frequency and -field electron paramagnetic resonance (HFEPR) and X-ray absorption spectroscopy (XAS). This panel of characterization is complemented by theoretical, electrochemical, and reactivity studies. We demonstrate how the Ti^{II} ion readily binds THF (reversibly) as well as N_2. In fact, coordination even of a strong σ base/π acid, such as CNAd (Ad = 1-adamantyl) to the Ti^{II} ion does not perturb the high-spin nature of the metal ion, despite forming a rare example of a five-coordinate isocyanide adduct, $[(Tp^{tBu,Me})TiCl(CNAd)]$. Last, we showcase how the Ti^{II} ion can be oxidized to Ti^{IV} to form platforms of the type $[(Tp^{tBu,Me})Ti{=}E(Cl)]$ (E^{2-} = O, $NSiMe_3$, N_2CPh_2, and NH).

RESULTS AND DISCUSSION

Synthesis of Mononuclear Ti^{III} Complexes with a Sterically Encumbering Trispyrazolylborate Ligand. Lee and co-workers reported how $[TiCl_2(TMEDA)_2]$ could be cleanly transmetalated with 2 equiv of [KTp] to afford the octahedral Ti^{II} complex $[TiTp_2]$. Intuitively, one would expect this reaction to proceed *via* the monomeric intermediate [TpTiCl]. Surprisingly, we found that no examples of mono-Tp-based Ti^{II} complexes exist, despite the V^{II} complex $[(Tp^{tBu_2})VCl]$ having been recently reported by Petrov and co-workers.[22] An initial investigation of salt metathesis between *mer*-$[TiCl_3(THF)_3]$ and $[KTp^{tBu_2}]$ led to isolation of the Ti^{III} complex $[(\kappa^1,\kappa^1,\eta^2\text{-}Tp^{tBu_2})TiCl_2]$, albeit in low (~10%) yield and with the presence of impurities (Scheme 1). Single-crystal X-ray diffraction (XRD; Figure 1) studies

Scheme 1. Synthesis of $[(\kappa^1,\kappa^1,\eta^2\text{-}Tp^{tBu_2})TiCl_2]$

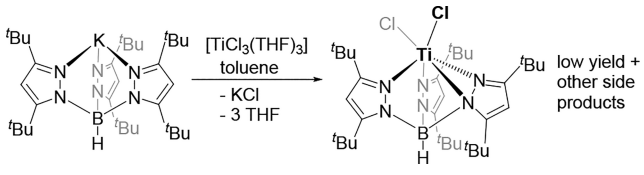

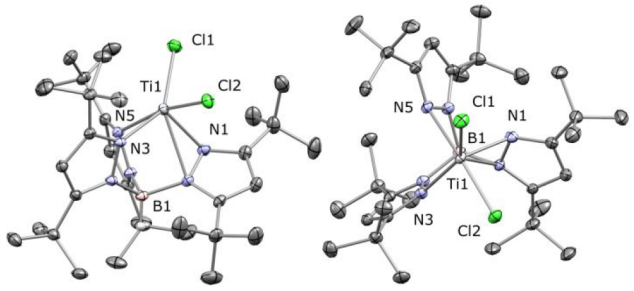

Figure 1. Two views of the solid-state structure of $[(\kappa^1,\kappa^1,\eta^2\text{-}Tp^{tBu_2})TiCl_2]$, showing distortion of one pyrazolyl arm of the Tp^{tBu_2-} ligand. Thermal ellipsoids are at 50% probability. Solvent and H atoms (except on B) are omitted.

revealed a highly distorted system where the Tp^{tBu_2-} ligand coordinates in an unusual κ^1,κ^1,η^2 mode, which has been observed only in coordination polymers[30] and for large metal ions that favor high coordination numbers, such as Ba^{II},[31] Sm^{III},[32] Yb^{II},[33] and U^{III}.[34] Here, the severe skewing of one pyrazolyl arm results in an almost side-on interaction between both of its N atoms and the metal ion. A moderate degree of elongation for one of the B−N bonds [B1−N2, 1.597(3) Å] compared to the other two [B1−N4 and B1−N6, 1.562(3) and 1.542(2) Å, respectively] can be observed. Consequently, the N−N distances in each ring reflect a subtle degree of activation of the pyrazolyl groups, with the side-on-bonded one possessing a longer distance [1.403(2) Å] compared to the other two [1.382(2) and 1.385(2) Å]. Distortion of one of the sterically encumbered pyrazolyl arms in $[(\kappa^1,\kappa^1,\eta^2\text{-}Tp^{tBu_2})TiCl_2]$ implies the possibility of decomposition reactions, involving B−N and N−N bond activation, especially in subsequent reduction chemistry, leading to the large and strongly reducing Ti^{II} ion. Not surprisingly, attempts to prepare pure samples of $[(\kappa^1,\kappa^1,\eta^2\text{-}Tp^{tBu_2})TiCl_2]$ invariably resulted in impure bulk material containing traces of other species, including free pyrazole. Given the larger ionic radius of Ti^{II} (100 pm) versus V^{II} (93 pm), we decided to reduce some of the steric congestion in Tp^{tBu_2-} by replacing the *tert*-butyl group in the 5 position of each pyrazolyl arm with a methyl group. Theopold and co-workers have popularized this ligand scaffold with various 3d metals, including the early-transition-metal Cr in the formal oxidation states I−V.[23,35]

Following a modified recipe to prepare $[(\kappa^1,\kappa^1,\eta^2\text{-}Tp^{tBu_2})TiCl_2]$, treatment of *mer*-$[TiCl_3(THF)_3]$ with 1 equiv of $[Tl(Tp^{tBu,Me})]$ in toluene over 13 h at 70 °C resulted in the smooth formation of $[(Tp^{tBu,Me})TiCl_2]$ (**1**), which was isolated in 72% yield as blue crystals (Scheme 2). The use of $[Tl(Tp^{tBu,Me})]$ as opposed to the K^+ salt improves the overall isolated yield because of the lower content of residual pyrazole that remains from synthesis of the alkali salt. X- and Q-band EPR spectroscopic studies of **1** in toluene glass afford typical $S = {}^1/_2$ rhombic spectra, indicative of low symmetry around the Ti^{III} ion (X band, g = [1.973, 1.923, 1.848], 12 K; Q-band, g = [1.973, 1.924, 1.848], 2 K; Figure 2). Likewise, solution Evans (μ_{eff} = 1.70 μ_B, 27 °C, C_6D_6), IR (ν_{BH} = 2569 cm^{-1}), and UV−vis (d−d, 648 nm; ε = 35 M^{-1} cm^{-1}) spectral studies are all in accordance with a monomeric d^1 species. While the starting material, *mer*-$[TiCl_3(THF)_3]$, shows a UV−vis absorption spectrum with two transitions due to a Jahn−Teller-distorted excited E_g state (668 and 763 nm, ε = 7 and 4 M^{-1} cm^{-1}, respectively), complex **1** shows a single transition at 648 nm with a 5-fold increase in intensity in accord with the lower

https://dx.doi.org/10.1021/acs.inorgchem.0c02586
Inorg. Chem. 2020, 59, 17834−17850

Scheme 2. Synthesis of Precursor 2 *via* Reduction of 1, Reactivity Studies Involving THF, N_2, CNAd, and Various Oxidants (N_2CPh_2, N_3SiMe_3, and N_2O), as Well as the Bicyclic Amine Hdbabh to Form the Parent Imide 7

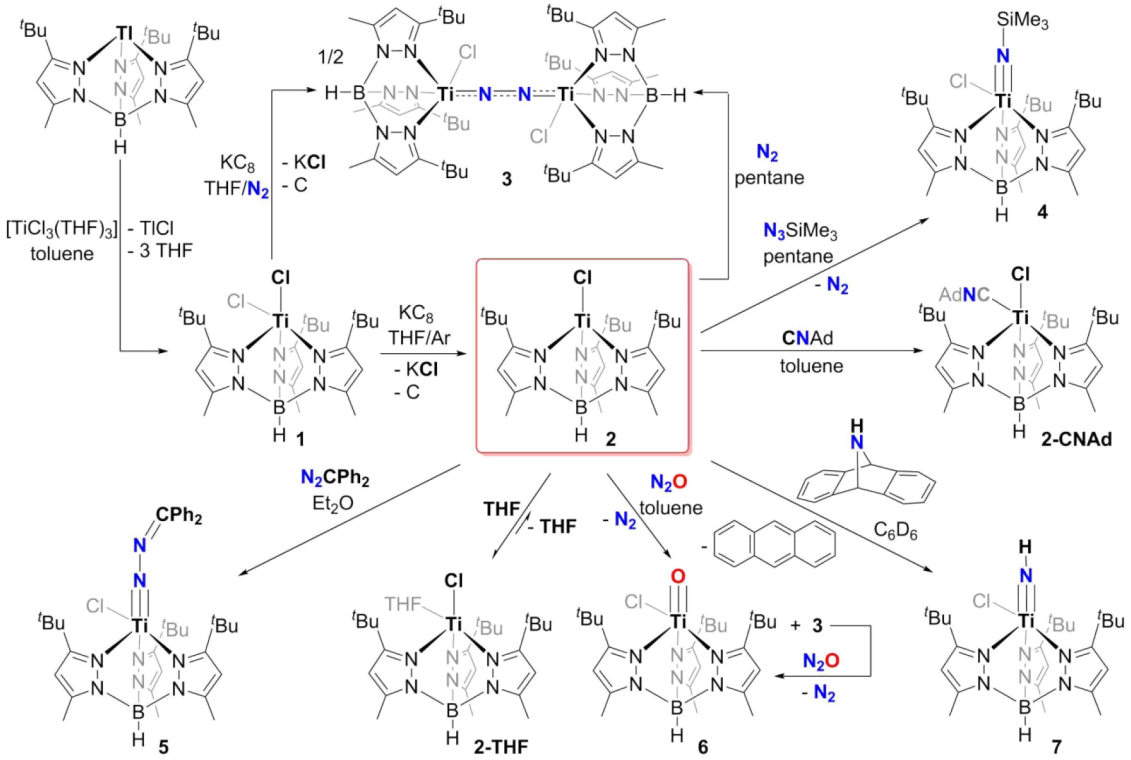

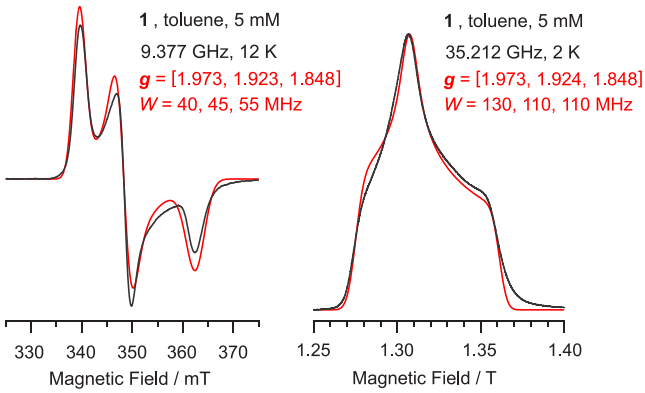

Figure 2. X-band (derivative, left) and Q-band (absorption, right) EPR spectra of **1** (black curves, experimental; red curves, simulated). Key experimental (black text) and $S = {}^1/_2$ powder pattern simulation (red text) parameters are given (W = Gaussian line widths, hwhm). The Q-band spectrum exhibits an absorption, rather than first derivative, line shape due to rapid passage effects.[38]

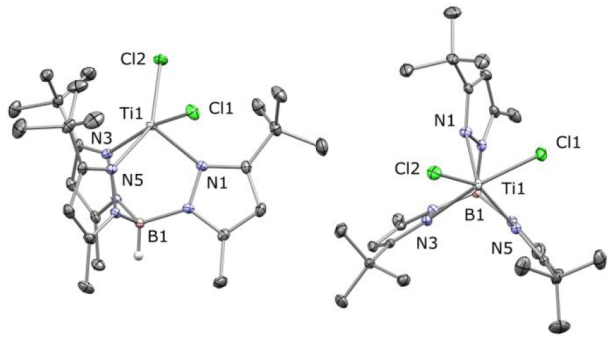

Figure 3. Solid-state structure of **1** from two different views. Thermal ellipsoids are at 50% probability. H atoms (except on B) are omitted.

symmetry about the Ti^{III} ion (Figure S51). XRD studies also confirmed a five-coordinate monomer more in line with a square-pyramidal geometry at the Ti^{III} ion ($\tau_5 = 0.27$;[36] Figure 3). Moreover, no isomeric species resulting from borotropic shifts[37] have been observed for **1**, and significant twisting of the pyrazolyl arms is no longer as noticeable when judged by the B−N and N−N metrical parameters. The view down the Ti−B−H axis (Figure 3, right) clearly shows how twisting of the pyrazole arms in **1** is minimized compared to $[(\kappa^1,\kappa^1,\eta^2\text{-}Tp^{tBu_2})TiCl_2]$.

Synthesis of a High-Spin, Tetrahedral Ti^{II} Complex and Exploration of Its Electronic Structure. A cyclic voltammogram of **1** revealed an irreversible one-electron anodic process with an anodic peak at 0.44 V (referenced to $FeCp_2^{0/+}$ as 0.0 V), while a reversible one-electron cathodic process could be observed at −1.85 V (Figure 4). In Lee's $[Tp_2Ti]PF_6$ complex, reversible one-electron oxidation and reduction processes occur at 1.20 and −1.28 V versus SCE, i.e., at 0.65 and −1.83 V versus $FeCp_2^{0/+}$.[39] These features indicate that reduction potentials are largely conserved between five-coordinate **1** and pseudooctahedral $[Tp_2Ti]PF_6$, and, importantly, both Ti^{III} complexes provide access to the corresponding Ti^{II} ions in a reversible manner. In the case of **1**, the nonreversible electrochemical features are likely due to significant structural distortion upon reduction, whereas the irreversible anodic feature might be due to the instability of a hypothetical four-coordinate $[\mathbf{1}]^+$ species, especially in the presence of electrolyte. Encouraged by the facile electrochemical reduction chemistry, we conducted a chemical reduction of **1** under Ar with KC_8 in THF over 10 min, which resulted in an immediate color change from blue to

https://dx.doi.org/10.1021/acs.inorgchem.0c02586
Inorg. Chem. 2020, 59, 17834−17850

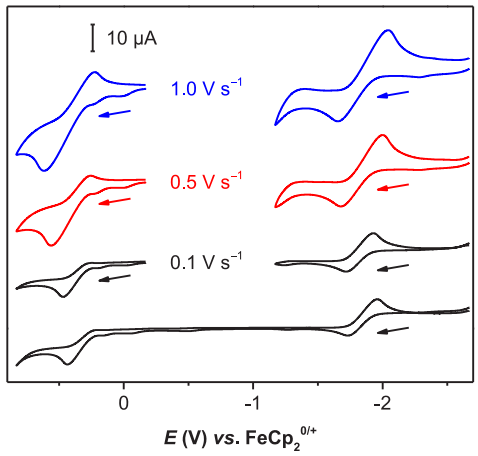

Figure 4. Scan-rate dependence for cyclic voltammograms of **1** under N_2 in 0.1 M $[^nBu_4N][PF_6]$ in THF.

intense green. Subsequent workup of the reaction mixture resulted in the formation of $[(Tp^{tBu,Me})TiCl]$ (**2**) as light-green crystals in a respectable yield (78%; ν_{BH} = 2554 cm^{-1}; Scheme 2). XRD studies revealed a slightly distorted tetrahedral Ti^{II} ion in each of the two crystallographically independent molecules (Table 1 and Figure 5, top). The chlorido ligand

Table 1. Geometric Parameters for the Two Crystallographically Independent Molecules of Complex 2 ($Pca2_1$)

geometry	τ_4/τ_δ	B−Ti−Cl(deg)	Ti−Cl (Å)	Ti−N_{avg} (Å)
2-lin	0.75/0.73	174.6(1)	2.375(2)	2.159
2-ben	0.69/0.57	162.9(1)	2.397(2)	2.180

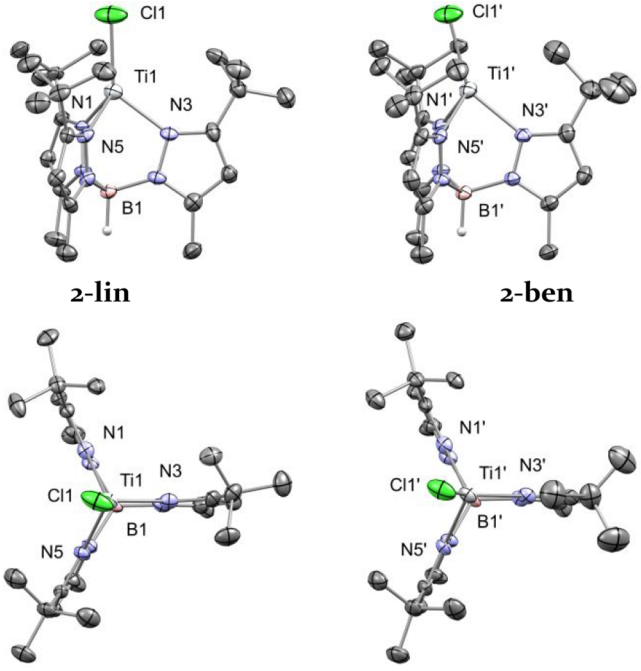

Figure 5. Solid-state structures of the two crystallographically independent molecules in **2** (left, **2-lin**; right, **2-ben**). Thermal ellipsoids are at 50% probability. H atoms (except on B) are omitted.

and Ti−B vector in the conformers of **2** range from being aligned in a nearly linear fashion (**2-lin**; τ_4 = 0.75 and τ_δ = 0.73[40]) to being significantly bent (**2-ben**; τ_4 = 0.69 and τ_δ = 0.57) with Cl−Ti−B = 174.6(1)° and 162.9(1)°, respectively. This tilt of the chlorido ligand has notable consequences on the solid-state electronic structure of **2** (Supporting Information, section 13). Figure 5 (bottom) shows the 3-fold axis along the Cl−Ti−B vector. As expected for the larger Ti^{II} ion, the average Ti−Cl distances in **2** exceed those in **1** (2.386 vs 2.307 Å), whereas the Ti−N distances remain practically unchanged (2.169 vs 2.178 Å). In fact, the Ti−Cl bonds in **2** fall within the longest 7% of crystallographically characterized Ti−Cl distances in the CSD (version 2020.1), reflecting the large size of the Ti^{II} ion in **2**. Solution (Evans, μ_{eff} = 2.72 μ_B, 27 °C, C_6D_6) and direct-current (dc) SQUID (μ_{eff} = 2.61 μ_B, 27 °C; Table 2) magnetization measurements of **2** are consistent with a high-spin Ti^{II} d^2 ion. Specifically, the SQUID magnetization measurements of **2** in the temperature range 2−300 K are consistent with an S = 1 species (for two independently isolated samples). Below 10 K, the magnetic moment drastically decreases to 2.24 μ_B (at 2 K), as shown in Figure 6, due to zero-field splitting (ZFS, *vide infra*). Variable-temperature and -field (VTVF) magnetization measurements between 1 and 5 T were also measured and simulated using a g_{avg} value of 1.85 (Figure 6, inset, and Table 2). Being confined to a tetrahedral coordination geometry, complex **2** shows ligand-field transitions at lower energies than those in **1**, extending into the near-IR (NIR) region of the UV−vis spectrum (λ = 391, 701, 857, 889, and 925 nm; ε = 1500, 180, 340, 320, and 230 M^{-1} cm^{-1}, respectively; Figure S52).

Given the unique geometry of **2** and the even number of unpaired electrons resulting in an integer electronic spin, we carried out HFEPR spectroscopic measurements of powdered samples of **2** at low temperatures (Figure 7, top, 216 GHz; spectra at additional frequencies are shown in Figures S59−S62). The spectra are characteristic powder patterns for a triplet spin state (S = 1) and reveal the presence of two independent S = 1 species. The number and intensity of turning points in the spectra could be readily simulated at various frequencies using two sets of spin-Hamiltonian parameters (Table 2). These parameters were obtained from 2D maps of field versus frequency (Figure 7, bottom), with a tunable-frequency methodology applied.[41] The sign of D was obtained from the simulation of single-frequency spectra such as those shown in Figure 7 and was found to be negative for one species, hence designated as **2-neg** and positive for the other, hence **2-pos** (E was assigned the same sign as that of D by convention). The spectroscopically determined D values compare well with the average value of the same parameter extracted from SQUID magnetometry (−5.08 cm^{-1}; Table 2), and the presence of two crystallographically independent molecules in the asymmetric unit of the crystal structure of **2** readily explains the two S = 1 species observed by HFEPR. Apparently, the sign and magnitude of D is highly sensitive to the geometry of the Ti^{II} ion in **2**. Ligand-field-theory (LFT) analysis using the angular overlap model provides an explanation for **2-neg** and **2-pos** having different magnitudes *and* signs of ZFS (Supporting Information, section 13). Conformer **2-lin**, which more closely approximates trigonal (C_{3v}) symmetry, is assigned to **2-pos**, whereas the more distorted conformer **2-ben** is assigned to **2-neg**.

The dependence of D on molecular structure was further explored by quantum-chemistry computational means. The **g** and **D** tensors were calculated for **2** by employing hybrid density functional theory (DFT) calculations using the B3LYP

https://dx.doi.org/10.1021/acs.inorgchem.0c02586
Inorg. Chem. 2020, 59, 17834−17850

Table 2. Electronic Structure Parameters for Complex 2 Extracted with SQUID Magnetometry and HFEPR Spectroscopy

			SQUID			
		D (cm^{-1})		E/D		g_{avg}
dc, 1 T		−5.08		0		1.85
VTVF		−4.86		0		1.85
			HFEPR			
species	D (cm^{-1})	E (cm^{-1})	E/D	g_x	g_y	g_z
2-pos	+1.55(1)	+0.38(1)	0.25	1.87(1)	1.89(1)	1.92(2)
2-neg	−5.91(2)	−0.31(2)	0.05	1.91(2)	1.94(2)	1.7(1)

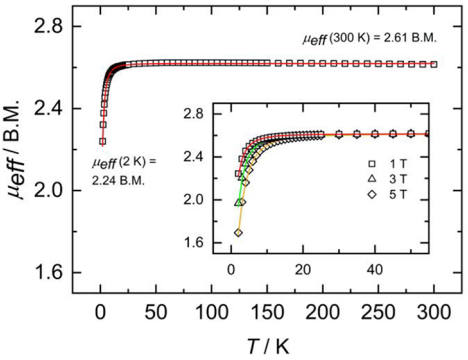

Figure 6. Solid-state dc and VTVF SQUID (inset) magnetization studies of **2** at 1−5 T from 2 to 300 K.

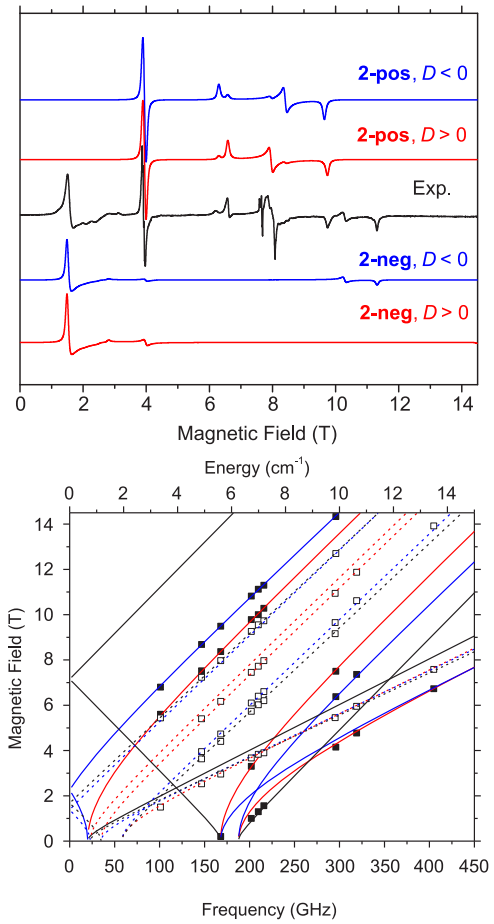

Figure 7. Top: Solid-state HFEPR spectrum of **2** at 4.5 K and 216 GHz (black trace). The colored traces are simulations using spin-Hamiltonian parameters (Table 2) of **2-neg** (bottom) and **2-pos** (top); red traces are simulations using positive D; blue traces are negative D values. Bottom: 2D plot of turning points in the powder spectra of **2** as a function of the frequency, marked as squares: full squares, **2-neg**; empty squares, **2-pos**. The lines are simulated with red color representing the turning points with the external magnetic field, B, parallel to the x axis of the zfs tensor, blue: $B \parallel y$, and black: $B \parallel z$.

hybrid density functional with the CP(PPP) basis set on the Ti atom and the ZORA-def2-TZVP(-f) basis set on all other atoms; the calculations were based on the atomic coordinates from the crystal structures. The two conformers of **2** (cf. Table 1) each gave a unique set of parameters, in accord with the appearance of two spin systems in the HFEPR data. Notably, as with classical LFT (Supporting Information, section 13), the calculations reproduce the oppositely signed D values, although the magnitudes of D and E/D poorly match the experimental data (Table 3), which was also the case using LFT. In light of this, complete-active-space self-consistent-field (CASSCF) calculations with the strongly contracted N-electron valence perturbation theory 2 (NEVPT2[42]) dynamical correlation correction were undertaken. Multiconfigurational approaches, including CASSCF/NEVPT2, predict ZFS for transition-metal complexes more accurately than DFT.[43] This is partially attributable to multiconfigurational methods giving a more accurate prediction of d−d excited-state energies, which are essential to accurately determining the spin−orbit coupling (SOC) contribution to the ZFS. The present calculations used the effective Hamiltonian theory and included both contributions from SOC and spin−spin coupling (SSC);[44] the SSC contribution is not directly accounted for in the classical LFT model.

The CASSCF/NEVPT2 calculations were based on the quasi-restricted orbitals (QROs[43d]) generated by the B3LYP calculation. The active spaces comprised two electrons and five orbitals [CAS(5,2)] and were averaged over all singlet (15) and triplet (10) ligand-field states expected for a d^2 ion in C_{3v} symmetry. State energies and ground-state configurations are included in the Supporting Information. The spin-Hamiltonian parameters (g, D, and E/D) calculated using this approach conform better with experiment than values calculated using DFT (Table 3). Importantly, species **2-neg** observed by HFEPR can be plausibly assigned to conformer **2-ben**, while **2-pos** can be assigned to conformer **2-lin**, exactly as proposed from LFT.

Reactivity of Complex 2 toward N_2, THF, and an Isocyanide. Transient Ti^{II} species are known to activate N_2, but reports of isolable and well-defined Ti^{II} species that can activate this inert gas remain quite rare.[8c,45] Potential synthetic applications of this activation chemistry include reductive splitting of N_2.[46] In order to prepare complex **2**, manipulations must be carried out under a strictly pure Ar atmosphere, and solvents must be sparged thoroughly in order to avoid

https://dx.doi.org/10.1021/acs.inorgchem.0c02586
Inorg. Chem. 2020, 59, 17834−17850

Table 3. Calculated Spin-Hamiltonian Parameters for Conformers of Complex 2

geometry	τ_4	method	g_1	g_2	g_3	D (cm^{-1})	E/D
2-lin/2-pos	0.75	DFT	1.966	1.971	1.973	−5.58	0.029
		CASSCF/NEVPT2[a]	1.792	1.829	1.916	+2.87	0.19
2-ben/2-neg	0.69	DFT	1.953	1.970	1.979	+7.59	0.020
		CASSCF/NEVPT2[a]	1.668	1.888	1.940	−7.77	0.068

[a]Calculated using CAS(2,5) with an effective Hamiltonian SOC contribution and including a SSC contribution. CASSCF calculations are state-averaged over all d−d states of the d^2 configuration.

reactivity with residual N_2. Indeed, we found that reduction of **1** with KC_8 in THF under a N_2 (as opposed to Ar) atmosphere, and with workup carried out essentially identically with that for **2**, resulted in the clean formation of a new diamagnetic product. Moreover, exposure of **2** in a pentane solution to an atmosphere of N_2 afforded the same species, quantitatively, over the course of minutes as a dark-green crystalline material. We should stress that, even in an Ar-filled glovebox, complex **2** gradually converts, in solution, to this new diamagnetic species, making it a potent scavenger of N_2! By contrast, crystalline **2** shows no signs of conversion into this new species when stored under N_2 over at least 24 h, reflecting the energetic penalties associated with structural changes in the solid state. The ^1H and ^{13}C NMR, in addition to IR (ν_{BH} = 2559 cm^{-1}), spectral data of this new species feature a single pyrazolyl chemical environment, indicating that the new five-coordinate species undergoes rapid Berry pseudorotations in solution. XRD studies established formation of the bridged N_2 species $[(Tp^{tBu,Me})TiCl]_2(\eta^1,\eta^1;\mu_2\text{-}N_2)$ (**3**) having a linear Ti═N═N═Ti topology (Scheme 2 and Figure 8). The

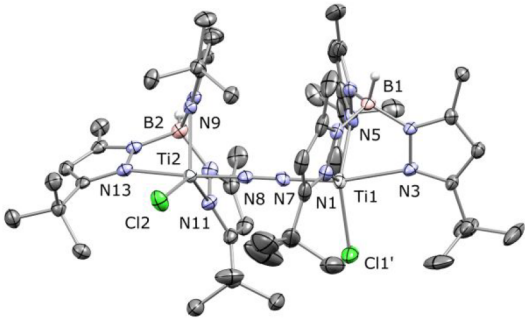

Figure 8. Solid-state structure of **3**. Thermal ellipsoids are at 50% probability. Solvent and H atoms (except on B) are omitted. Disorder in two ^{t}Bu groups and Cl1′ is not shown.

elongated N−N bond of 1.207(4) Å with respect to free N_2 (1.0977 Å),[47] the short Ti−N distances [1.805(3) and 1.812(3) Å], and the diamagnetic nature hints to this motif being somewhere in the N_2^{2-} range. The two Cl ligands are oriented with dihedral angles of 85.43(7)−115.98(5)° (one Cl is disordered), consistent with complex **3** adopting both gauche and eclipsed conformations in the solid state. Dark-green **3** absorbs strongly across the entire UV−vis region with a maximum at 652 nm (ε = 580 M^{-1} cm^{-1}; Figure S55), reflecting strong interaction between the bridging N_2 ligand and Ti centers.

Returning to the Ti^{III}/Ti^{II} redox couple from the electrochemical studies of **1**, it would be interesting to establish whether the identity of the reduced species might correspond to **2** or **3**. During the synthesis of **2** and **3**, we noted that the reduction of **1** with KC_8 in THF, in both cases, afforded an intense-green solution, the color of which matches neither the light-green color of **2** nor the dark-green color of **3**. In both syntheses, removal of the volatiles produces an intense-green film, and the addition of pentane induces crystallization of **2** (under Ar) and **3** (under N_2) over the course of minutes. Surprisingly, an initial attempt at generating the ^{15}N isotopologue of **3** by exposing **2** to $^{15}N_2$ in THF over 1 h resulted in the isolation of only unconverted **2**. Likewise, a complementary experiment involving the reduction of **1** with KC_8 in THF under N_2, followed by removal of the volatiles *in vacuo* and subsequent workup under Ar, afforded a mixture of **2** and **3** in a 70:30% proportion. To better understand the apparent inhibition of N_2 binding to **2** in THF, we turned to UV−vis spectroscopic studies. Upon going from toluene to a THF solution, absorption from **2** at 391 nm (1500 M^{-1} cm^{-1}) undergoes a slight redshift to 412 nm (380 M^{-1} cm^{-1}). More importantly, the intense absorptions extending into the NIR region (λ = 701, 857, 889, and 925 nm and ε = 180, 340, 320, and 230 M^{-1} cm^{-1}, respectively) disappear altogether and are replaced by a weaker and broad absorption at 606 nm (38 M^{-1} cm^{-1}; Figure S53). Thus, titration of toluene solutions of **2** with THF (0−0.70 M) indicates that an equilibrium takes place between **2** and the Lewis base with an association constant in the range of 5−8 M^{-1} (Figure 9, left). In neat THF

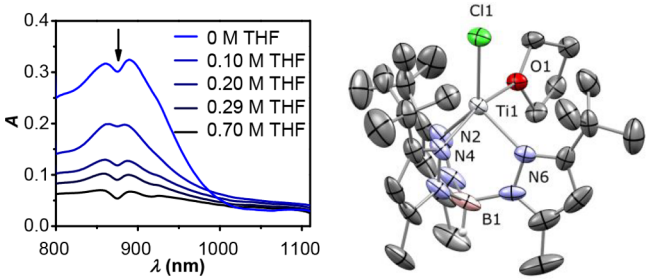

Figure 9. Left: UV−vis absorption spectra of **2** (1.6 mM) in toluene with increasing concentrations of THF. Right: Solid-state structure of **2-THF**. Thermal ellipsoids are at 50% probability. Solvent and H atoms (except on B) are omitted.

(12.3 M), this corresponds to 98−99% of **2** being present as the five-coordinate $[(Tp^{tBu,Me})TiCl(THF)]$ (**2-THF**; Scheme 2 and Figure 9, right). Eventually, we isolated crystalline **2-THF** (in the strict absence of N_2) by prolonged storage of **2** in pentane containing low concentrations of THF (−35 °C). XRD studies verify that **2-THF** is a rare example of a five-coordinate, mononuclear, and high-spin Ti^{II} ion (τ_5 = 0.46). Moreover, the Ti−Cl [2.414(1) Å] and Ti−O_{THF} [2.251(2) Å] distances in **2-THF** fall in the longest decile of crystallographically characterized Ti−Cl and Ti−O_{THF} distances in the CSD (version 2020.1), again reflecting the size of the Ti^{II} ion in **2-THF**. Importantly, the reactivity and spectroscopic and structural data provide evidence that the

https://dx.doi.org/10.1021/acs.inorgchem.0c02586
Inorg. Chem. 2020, 59, 17834−17850

reduction of **1** to ultimately produce **2** or **3** proceeds with **2-THF** as a common intermediate (Scheme 2). It is apparent from our studies that THF blocks the binding site for N_2 activation. This finding is quite influential because it suggests that reductions of metal ions, often conducted in polar solvents such as THF, might actually disfavor binding of N_2 if the association constant of THF is large. In addition to this feature, the lability of the THF ligand is central for the Ti^{II} ion in subsequently attaining the tetrahedral geometry that is characteristic of complex **2**.

Exposing complex **2** to isotopically enriched $^{15}N_2$ in pentane afforded $[(Tp^{tBu,Me})TiCl]_2(\eta^1,\eta^1;\mu_2\text{-}^{15}N_2)$ (**3**-^{15}N), and collecting ^{15}N NMR spectroscopic data revealed a downfield chemical shift at 309 ppm [vs NH_3(l) referenced at 0.0 ppm; top right in Figure 10]. The ^{15}N NMR data indicate a

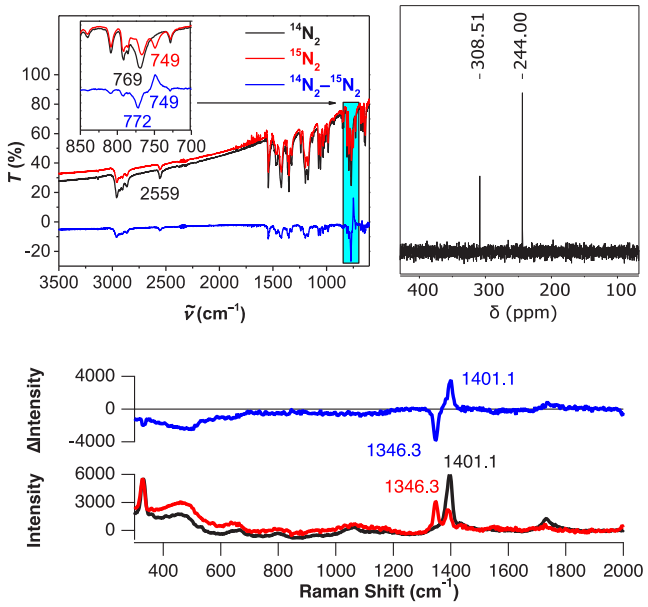

Figure 10. Top left: IR spectral data for **3** (black) and **3**-^{15}N (red) along with a difference spectrum (blue). Top right: ^{15}N NMR spectrum of **3**-^{15}N [with an external standard, AdC^{15}N, referenced at 244 ppm vs NH_3(l) referenced at 0.0 ppm[49]]. Bottom: Resonance Raman (405 nm excitation) data for **3** (black) and **3**-^{15}N (red) along with a difference spectrum (blue).

reduced N_2 ligand; known $[\{L_nTi\}_2(\eta^1,\eta^1;\mu_2\text{-}^{15}N_2)]$ complexes display ^{15}N resonances in the range of 322–558 ppm versus NH_3(l).[7h,i,k,l] A comparison of the IR spectra of **3**-^{15}N and **3** allows the identification of low-energy Ti–N stretching frequencies ($^{14}N/^{15}N$ at 769/749 cm^{-1}; Figure 10, top left), which gives a ratio (1.027) in good agreement with that calculated within the harmonic oscillator approximation for a $^{48}Ti–^{14}N/^{48}Ti–^{15}N$ isotopic system (calcd 1.0269). Resonance Raman spectroscopy obtained by excitation at 405 nm reveals a strongly red-shifted N–N vibration ($^{14}N/^{15}N$ at 1401.1/1346.3 cm^{-1}; Figure 10, bottom), indicating a highly reduced N_2 unit consistent with a N_2^{2-} ligand (informative N–N Raman stretching frequencies;[48] N_2H_4, 1076 cm^{-1}; *trans*-N_2H_2, 1529 cm^{-1}). With these data, **3** can be formally construed as two Ti^{III} ions bridged by a N_2^{2-} ligand.

We also investigated the reactivity of **2** with a π acid, such as the isocyanide CNAd, to probe whether this reaction would yield a low-spin complex. Accordingly, treatment of **2** with CNAd resulted in clean formation of the adduct $[(Tp^{tBu,Me})$-TiCl(CNAd)] (**2-CNAd**) in 66% yield as a dark-maroon crystalline material. The ^{1}H NMR spectrum of **2-CNAd** covers a ~50 ppm chemical shift range (−8 to +40 ppm), similar to the range found for **2** (−2 to +46 ppm). Likewise, the magnetic moment extracted with Evans' method (μ_{eff} = 2.72 μ_B, 28 °C, C_6D_6) attests to **2-CNAd** still being high spin, consistent with the persistence of a Ti^{II} ion. Akin to **2-THF**, an XRD study reaffirmed the connectivity in **2-CNAd**, showing a rare example of a five-coordinate high-spin Ti^{II} complex (Figure 11). The linear Ti–C–N geometry [174.2(1)°] in **2-**

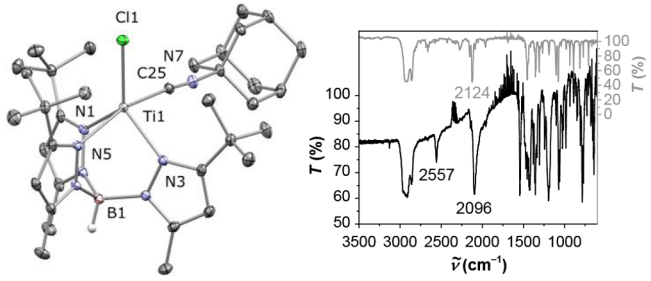

Figure 11. Left: Solid-state structure of **2-CNAd**. Thermal ellipsoids are at 50% probability. Solvent and H atoms (except on B) are omitted. Right: IR spectral data of **2-CNAd** (black) and free CNAd (gray).

CNAd and the modest redshift of the C≡N stretching frequency versus free CNAd (2096 vs 2124 cm^{-1}; Figure 11) reflect a moderate degree of π-back-bonding, in line with the high-spin nature of **2-CNAd**. However, the isonitrile ligand is not entirely spectroscopically innocent because the UV–vis spectrum of **2-CNAd** displays much more intense charge-transfer bands (λ < 450 nm and ε > 3000 M^{-1} cm^{-1}; Figure S56) than complexes **2** and **2-THF**.

XAS Spectra of Complexes 1–3 and 2-CNAd. Ti K-edge XAS spectra were obtained for compounds **1**–**3** and the titanium(II) isocyanide adduct, **2-CNAd** (Scheme 2 and Figure 12). The rising-edge energies obtained from the first

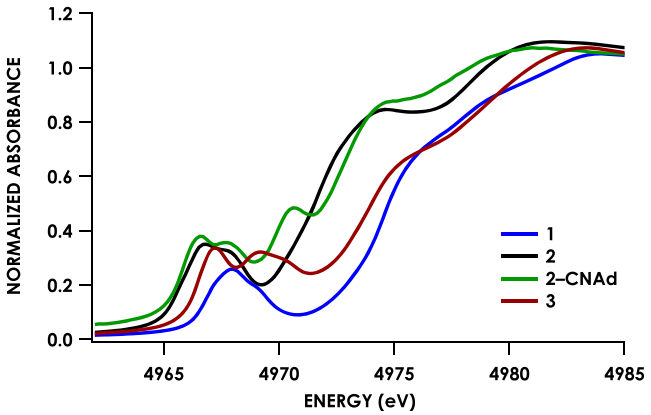

Figure 12. Ti K-edge XAS data for complexes **1** (blue), **2** (black), **2-CNAd** (gray), and **3** (red).

derivatives of the spectra are presented in Table 4. Compounds **1** and **3** exhibit inflection points at 4974.5 and 4973.9 eV, respectively, while **2** and **2-CNAd** have inflection points at 4971.6 and 4971.1 eV, respectively. The ca. 3 eV gap between the pairs of rising-edge energies accords with the assignment of **2** and **2-CNAd** as *bona fide* Ti^{II} species, whereas **1** and **3** are

https://dx.doi.org/10.1021/acs.inorgchem.0c02586
Inorg. Chem. 2020, 59, 17834–17850

Table 4. Ti K-Edge XAS Preedge and Rising-Edge Energies for 1−3 and 2-CNAd

complex	preedge energy (eV)	rising-edge energy (eV)
1	4968.0	4974.5
2	4966.8	4971.6
2-CNAd	4966.6	4971.1
3	4967.3	4973.9

physically defined Ti^{III} species. The XAS spectra also display prominent preedge absorption features, which were assigned with aid from time-dependent density functional theory (TDDFT) calculations (*vide infra*).

Electronic Structure Calculations. Hybrid DFT calculations using the B3LYP hybrid density functional with the CP(PPP) basis set on the Ti atom and the ZORA-def2-TZVP(-f) basis set on all other atoms were carried out using atomic coordinates from the crystal structures. The calculations were used as starting points for TDDFT calculations of the Ti K-edge XAS data. Calculated excitation energies correlated strongly and linearly with the experimental data (Figure S66; R^2 = 0.97). The linear fit was used to shift the calculated energies such that the calculated and experimental spectra overlap (Figures 13 and 14). Spectra for **2** were calculated for both independent conformers in the crystal structure (**2-lin** and **2-ben**; Table 1) but were found to be effectively superimposable.

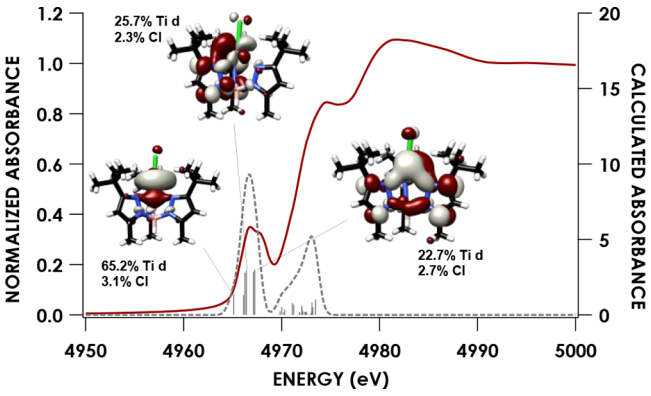

Figure 13. Overlap of the experimental and TDDFT-calculated [B3LYP and CP(PPP) on the Ti atom and ZORA-def2-TZVP(-f) on all other atoms] Ti K-edge XAS spectra of **2** (geometry for conformer **2-lin**) with acceptor MOs for preedge transitions plotted at an isovalue of 0.03 au. Calculated data have been energy-shifted following the correlation given in Figure S66.

Assignments of the preedge features in the Ti K-edge XAS data of **2** and **3** were facilitated using molecular orbital (MO) diagrams produced by the initial single-point DFT calculations. Complex **2** exhibits a 2 + 1 + 2 d−d splitting diagram, as would be expected for an effectively C_{3v} system (Figure 15). The two d electrons reside within an effectively degenerate (e) level comprised of MOs of ca. 80% d character in accordance with the physical Ti^{II} d^2 assignment suggested by the XAS data. Preedge excitations thus comprise several quadrupole-allowed Ti 1s → 3d excitations that gain intensity due to 4p mixing in the C_{3v} environment.

The MO diagram of **3** (Figure 16) resulting from a spin-restricted hybrid DFT calculation depicts four electrons in two pseudodegenerate MOs of ∼50% Ti 3d and ∼30% N 2p

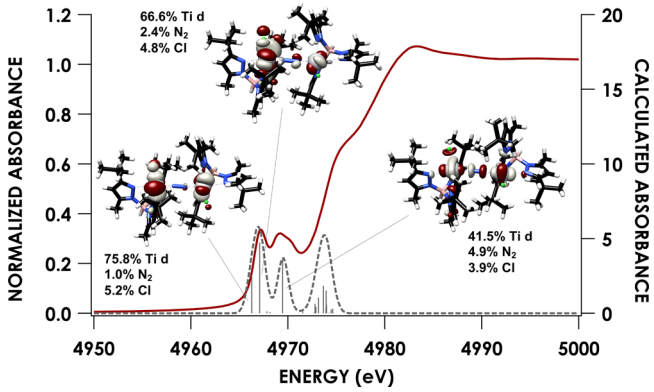

Figure 14. Overlap of the experimental and TDDFT-calculated [B3LYP and CP(PPP) on the Ti atom and ZORA-def2-TZVP(-f) on all other atoms] Ti K-edge XAS spectra of **3** with acceptor MOs for preedge transitions plotted at an isovalue of 0.03 au. Calculated data have been energy-shifted following the correlation given in Figure S66.

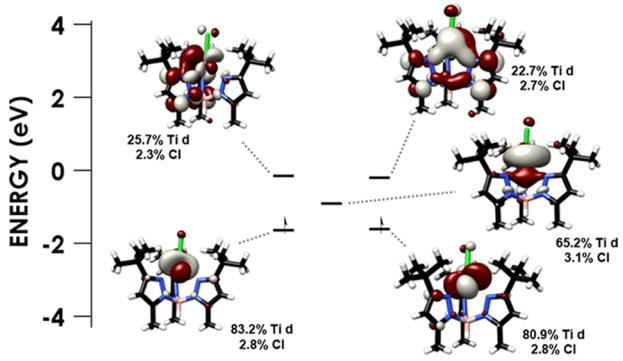

Figure 15. Truncated MO diagram depicting the ligand field for **2** (geometry for conformer **2-lin**) using QROs generated following a spin-unrestricted (UKS) DFT calculation using the B3LYP hybrid density functional with the CP(PPP) basis set on the Ti atom and the ZORA-def2-TZVP(-f) basis set on all other atoms. Orbitals are plotted at an isovalue of 0.03 au.

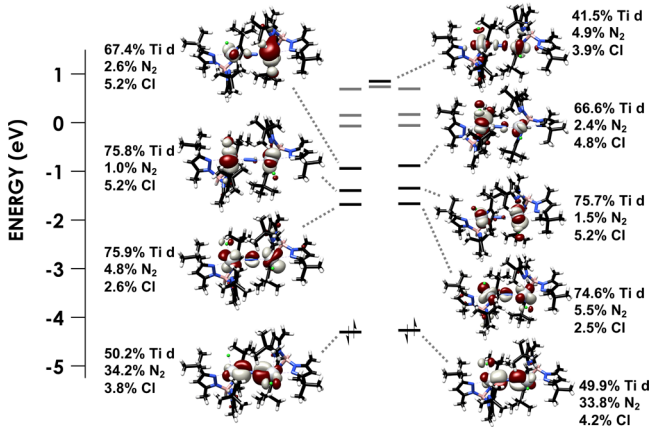

Figure 16. Truncated MO diagram for **3** generated with a spin-restricted hybrid DFT calculation employing the B3LYP hybrid density functional, the CP(PPP) basis set on the Ti atom, and the ZORA-def2-TZVP(-f) basis set on all other atoms. Orbitals in black have large contributions from Ti 3d, while orbitals in gray have small (<10%) contributions from Ti 3d. Orbitals are plotted at an isovalue of 0.03 au.

https://dx.doi.org/10.1021/acs.inorgchem.0c02586
Inorg. Chem. 2020, 59, 17834−17850

parentages. An alternative electronic structure description for **3** involves the antiferromagnetic coupling of two Ti^{III} ions through the N_2 bridge. To explore these bonding scenarios, we carried out broken-symmetry (BS1,1) calculations on **3**. However, unrestricted corresponding orbital analysis reveals that no pairs of α and β spin orbitals have low overlap ($S < 0.75$). Two pairs of spin orbitals have intermediate overlap ($S \sim 0.8$); these are π-bonding combinations between two Ti 3d and two N 2p orbitals, which are effectively delocalized over the entire $(Ti_2N_2)^{4+}$ fragment. Moreover, the calculated coupling constant[50] is $J \sim -5000\ cm^{-1}$, an excessively large magnitude to be considered magnetic exchange. Together, these values suggest that considering **3** as a pair of Ti^{III} centers antiferromagnetically coupled through the bridging N_2 fragment is inappropriate. Instead, the crystallographic, spectroscopic, and computational data for **3** are in line with a $Ti^{III}-N_2^{2-}-Ti^{III}$ core having two covalent bonds between N_2 and two Ti.

Reactivity of Complexes 2 and 3 toward Small Molecules. Complex **2** is stable in the solid state at room temperature and can be stored over months without showing signs of decomposition. In a toluene or benzene solution, **2** is stable over several hours at room temperature, after which it degrades to a myriad of unrecognizable diamagnetic products (full degradation after 20 h). By contrast, **2** is stable for at least 24 h in a THF solution at room temperature (by forming **2-THF**), reflecting the increase in stability achieved upon attainment of a five-coordinate geometry (*vide supra*). Complex **2** displays rich chemistry; for example, it rapidly reacts with N_3SiMe_3 to form the imide $[(Tp^{tBu,Me})Ti{\equiv}NSiMe_3(Cl)]$ (**4**) in 80% isolated yield along with N_2 extrusion (Scheme 2). Complex **4** is diamagnetic and has been characterized by a combination of IR and ^1H and ^{13}C NMR spectra in addition to solid-state structural studies (Figure 17, top left). ^{29}Si NMR spectroscopy reveals an upfield resonance (−13.5 ppm, vs $SiMe_4$ referenced at 0.0 ppm), indicating that the "$(Tp^{tBu,Me})Ti{\equiv}N^-(Cl)$" fragment in **4** is more electron-donating than a methyl group. The structure shows short Ti−N distances for the imide ligand [1.692(1)−1.700(2) Å] in accordance with metal−ligand multiple-bond character, whereas the Ti−N−Si angles [158.94(10)−160.24(9)°] indicate that the imide N is best described as an sp-hybridized motif. In contrast, when **2** is treated with N_2CPh_2, N_2 is not expelled, and instead of the hypothetical carbene "$[(Tp^{tBu,Me})Ti{=}CPh_2(Cl)]$", the diamagnetic diazoalkane adduct $[(Tp^{tBu,Me})Ti{\equiv}NNCPh_2(Cl)]$ (**5**) is isolated in 91% yield. Neither thermolysis (100 °C, overnight) nor photolysis (full spectrum from a Xe lamp, 1 h) promotes N_2 extrusion from **5**. Thus, **5** behaves like Herberhold's prototypical $[Cp_2Ti(N_2CPh_2)(PMe_3)]$ complex[51] but shows marked contrast to the more reactive $[Cp_2Ti(diazoalkane)]$ systems studied by Bergman, Andersen, and Chirik.[52] While **4** shows C_s symmetry in solution (two sets of pyrazole resonances), **5** displays a symmetry similar to that of **3** in solution, based on multinuclear NMR spectral studies, reflecting the larger separation between the CPh_2 and ^{t}Bu groups in **5** compared to the $SiMe_3$ and ^{t}Bu groups in **4**. A solid-state structure confirmed retention of the N_2 unit in **5**, as well as the presence of a short Ti−N multiple bond [1.722(1) Å; Figure 17, top right]. Bond distances within the diazoalkane ligand in **5** [C−N, 1.297(2) Å; N−N, 1.327(2) Å] correspond reasonably well with bond distances in the hydrazone, Ph_2CNNH_2 [C−N, 1.286(2) Å; N−N, 1.371(3) Å].[53] This

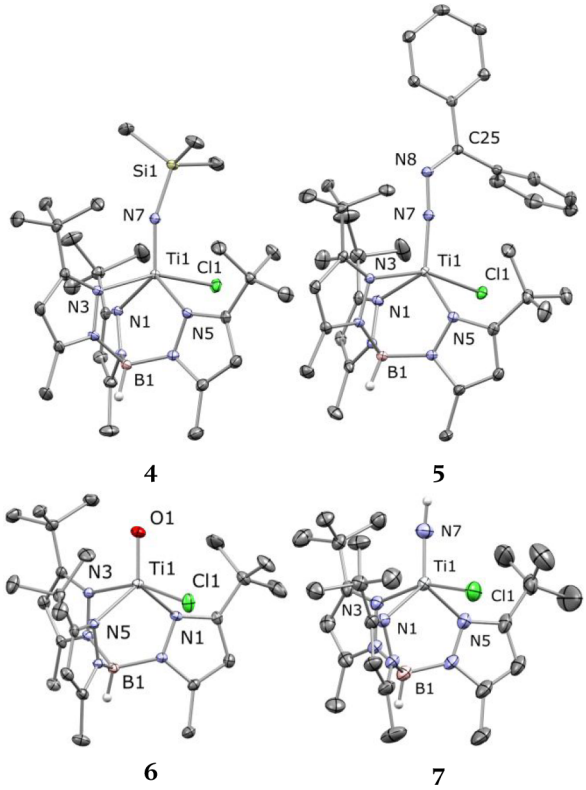

Figure 17. Top: Solid-state structures of **4** (two polymorphs with two and three crystallographically independent molecules, respectively) and **5**. Bottom: Solid-state structures of **6** and **7** (two crystallographically independent molecules). Thermal ellipsoids are at 50% probability. Solvent and H atoms (except on B and N) are omitted.

hints at a dianionic diazoalkane ligand; notably, free diaryldiazoalkanes display much shorter N−N bond distances (1.12−1.16 Å).[54]

We also explored the reactivity of the high-spin, tetrahedral Ti^{II} ion in **2** with other small molecules. N_2O reacts immediately upon contact with a benzene solution of **2** to form the terminal oxo $[(Tp^{tBu,Me})Ti{\equiv}O(Cl)]$ (**6**) along with **3** (Scheme 2), due to the concomitant release of N_2 and trapping by 2 equiv of the azophile **2**. The greater affinity of **2** for N_2 than N_2O most likely results in capture of the former. However, one could also argue for a bimolecular mechanism[55] involving a N_2O complex,[56] "$[(Tp^{tBu,Me})Ti(N_2O)(Cl)]$", reacting with **2**. Regardless, the reaction mixture progresses over 18 h to eventually form the oxo complex in quantitative spectroscopic yield, and workup results in colorless crystals of **6** in 75% isolated yield (Scheme 2). Independently, treating **3** with 1 atm of N_2O cleanly produces **6**, thus rendering the former species a masked form of Ti^{II} ion.[8e,57] The Ti≡O bond in **6** is remarkably short [1.621(1) Å; Figure 17, bottom left], possibly in line with triple-bond character; this is also manifested in the ^1H NMR spectrum of **6**, where the Me and ^{t}Bu groups display broad resonances because of restricted rotation (e.g., *via* a Berry pseudorotation) around the central Ti≡O unit. This feature might contribute to the more restricted rotation in **4** compared to **3** and **5**, but it is noteworthy that the ^1H NMR spectrum of **7** (a titanium imide akin to **4**, *vide infra*) shows only a single pyrazole environment.

The bicyclic amine 2,3:5,6-dibenzo-7-azabicyclo[2.2.1]-hepta-2,5-diene (Hdbabh)[58] delivers a parent imide moiety to the Ti^{II} ion of **2** by forming $[(Tp^{tBu,Me})Ti{\equiv}NH(Cl)]$ (**7**) in

https://dx.doi.org/10.1021/acs.inorgchem.0c02586
Inorg. Chem. 2020, 59, 17834−17850

near-quantitative spectroscopic yield (Scheme 2). Separation of **7** from the side product anthracene can be achieved *via* filtration of the reaction mixture through activated charcoal, providing yellow crystals of **7** in 32% isolated yield. The $^{1}H-^{15}N$ HSQC NMR spectrum of **7** unambiguously identifies the parent imide group through a cross-peak between a ^{1}H triplet (4.97 ppm) and a downfield ^{15}N nucleus (458 ppm; Figure S36). The same conclusion can be derived from the IR spectrum of **7**, which exhibits a strong NH stretching vibration (3296 cm^{-1}). Whereas terminal titanium−oxo ligands are not uncommon, terminal parent imides are quite a rare motif for group 4 transition metals.[59] A solid-state structural study of **7** (Figure 17, bottom right) confirms the terminal parent imide motif and a geometry similar to that of **4** and **6**. The imide H for both independent molecules was located in the difference Fourier map, and the Ti−N bond distances [1.674(4)−1.680(4) Å] fall within the range for terminal titanium imide complexes [1.627(8)−1.747(2) Å].[59a−d] The transfer of a parent imide group to low-valent Ti, thereby forming a mononuclear group 4 transition-metal imide, is unprecedented. In a few instances, this type of reaction has been reported for group 5 metals, *via* NH group transfer from 2-methylaziridine to V^{III} and Ta^{III} ions.[60] Moreover, NH transfer reactions from aziridines or Hdbabh are known to generate transient imide functionalities, which are implicated in the formation of amide and nitride complexes of Ti, W, and Fe.[61] The few known examples of titanium complexes having the parent imide group have been reported by several routes: deprotonation of NH_3,[59a] protonation of a nitride salt,[59d] or *via* a nitridyl radical that effects H-atom abstraction[59b,c] Along these lines, an alternative, nitridyl-mediated, route to **7** consists of treatment of the Ti^{III} precursor **1** with NaN_3 in THF. However, this reaction suffers from the sacrificial use of the [$Tp^{tBu,Me}$Ti] fragment as a H-atom source as well as the partial substitution of chloride for azide, thus giving mixtures of the corresponding azide and chloride imide complexes [($Tp^{tBu,Me}$)-Ti≡NH(X)] [X^{-} = N_3 or Cl (**7**)] as well as other poorly defined decomposition products. The azide imide complex was identified *via* the characteristic ^{1}H NMR resonance from the NH group (triplet at 3.58 ppm; Figure S33).

With the availability of structural and vibrational data for the new complexes **1**, **2**, adducts of **2**, and the derived products (**3**−**7**), some general conclusions about their geometries and electronic structure can be inferred (Table 5). With **1** as the exception (τ_5 = 0.27), the values of τ_5 fall closely around 0.5, such that complexes **2-THF**, **2-CNAd**, and **3**−**7** do not lend themselves to a classification as being either trigonal-bipyramidal or square-pyramidal. The divalent nature of **2-THF** and **2-CNAd** can be directly seen from the long Ti−E and Ti−Cl distances compared to complexes **3**−**7**, both reflecting the single-bond character of the Ti−E bonds and the large size of the Ti^{II} ion. Complexes **2-THF**, **2-CNAd**, and **3**−**7** underline the strong tendency for complex **2** to undergo reactions that render the Ti ion five-coordinate. As the reverse to this, complexes **4** and **7** might, in principle, eliminate small molecules (Me_3SiCl and HCl) to generate a neutral titanium nitride functionality, but this mode of reactivity is not operational for the ($Tp^{tBu,Me}$)Ti≡E(Cl) scaffold. Finally, inspection of the molecular structures of all complexes reported herein shows that the Ti^{II} complexes have Ti−Cl and B−H vectors oriented in an antiparallel fashion, whereas the Ti^{IV} complexes have the same vectors aligned nearly perpendicular. Indeed, the average B−Ti−Cl angles correlate well with the average Ti−B separations, as shown in Figure 18,

Table 5. Geometric Parameters and Vibrational Spectroscopic Data for Five-Coordinate Complexes 1, 2-THF, 2-CNAd, and 3−7

complex	E	τ_5	Ti−Cl (Å)	Ti−E (Å)	ν_{BH} (cm^{-1})
1		0.27	2.2816(6)−2.3310(6)		2569
2-THF	O	0.46	2.414(1)	2.251(2)	
2-CNAd	C	0.54	2.4123(5)	2.207(1)	2557
3	N	0.46−0.50	2.317(2)−2.360(2)	1.805(3)−1.812(3)	2559
4	N	0.46−0.59	2.3440(6)−2.3567(6)	1.692(1)−1.700(2)	2542
5	N	0.48	2.3486(4)	1.722(1)	2545
6	O	0.54	2.3468(6)	1.621(1)	2554
7	N	0.46−0.50	2.340(1)−2.348(1)	1.674(4)−1.680(4)	2543

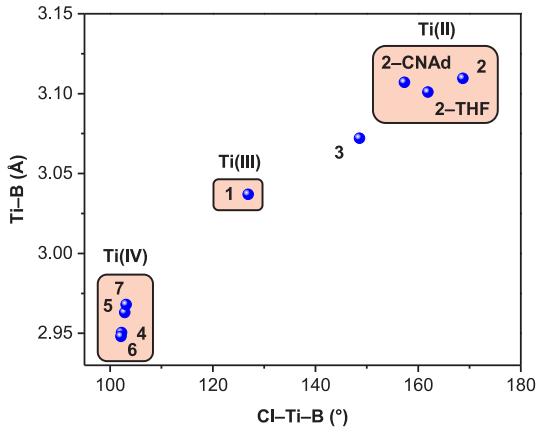

Figure 18. Average Ti−B distances versus Cl−Ti−B angles for the Ti complexes reported herein, representing formal oxidation states II−IV.

revealing that all complexes group into three distinct regions when judged by their formal oxidation states. The link between metric variation and the formal oxidation state likely reflects the increasing ionic radius encountered upon going from Ti^{IV} to Ti^{II}; thus, a reduced Ti center tends to slide out of the $Tp^{tBu,Me-}$ ligand, accounting for the increase in Ti−B separations and the straightening of B−Ti−Cl angles. Importantly, complex **3** falls between the Ti^{II} and Ti^{III} regions in Figure 18, augmenting support for the assignment of **3** as consisting of two Ti^{III} centers covalently bound through an N_2^{2-} ligand.

CONCLUSIONS

In summary, we have demonstrated the use of a sterically encumbering tris(pyrazolyl)borate ligand, $Tp^{tBu,Me-}$, to generate the Ti^{III} precursor, **1**. Tuning of the steric profile of the Tp ligand (replacement of the 5-^{t}Bu group with Me) proved essential for obtaining a Ti^{III} precursor with sufficient purity and stability for subsequent chemistry. Reduction of **1** under Ar furnishes a new geometry with a unique electronic structure: a stable tetrahedral Ti^{II} ion, **2**, having two unpaired electrons. The Ti K-edge XAS spectrum of **2** is shifted to lower energy relative to structurally similar complexes bearing

https://dx.doi.org/10.1021/acs.inorgchem.0c02586
Inorg. Chem. 2020, 59, 17834−17850

formally Ti^{III} centers, consistent with **2** having a more reduced metal center. Complex **2** exhibits a $^3A_2$ electronic ground state because of its confinement to a tetrahedral coordination geometry, as demonstrated by the magnetic moments extracted from SQUID magnetometric studies; the spin-only d^2 behavior of **2** persists to temperatures as low as 10 K, whereupon ZFS results in a drastically lowered magnetic moment. HFEPR spectroscopic studies corroborate that **2** is a *bona fide* example of an $S = 1$ Ti^{II} ion *via* the observation of two spin triplet systems (ZFS parameters: $D = -5.91$ and $+1.55$ cm^{-1}, respectively). The origin of two $S = 1$ systems can be traced to the two crystallographically independent molecules (conformers) in **2**, which display geometric distortions around the tetrahedral Ti^{II} ion, e.g., B−Ti−Cl angles spanning 162.9(1)−174.6(1)°. This assertion is supported by classical LFT and by CASSCF/NEVPT2 calculations, which closely reproduce these ZFS parameters and depict excited-state manifolds consistent with d^2 ions in an effective C_{3v} environment. Complex **2** is a potent scavenger of N_2, thus producing the dinuclear diamagnetic complex **3**, where the N_2 unit coordinates in a linear fashion between two Ti centers. The use of $^{15}N_2$ to generate isotopically labeled **3**-$^{15}N_2$ confirms atmospheric N_2 as the source of the bridging N_2 ligand. Labeling studies further identify a N−N stretching frequency by Raman spectroscopy ($^{14}N/^{15}N$ at 1401.1/1346.3 cm^{-1}), a Ti−N stretching frequency by IR vibrational spectroscopy ($^{14}N/^{15}N$ at 769/749 cm^{-1}), and a ^{15}N NMR resonance at 309 ppm. Ti K-edge XAS supported by TDDFT calculations accord with these complexes bearing physically defined Ti^{III} d^1 centers. Taken together, these results show that the bonding in **3** can be viewed as a covalent interaction between two Ti centers and N_2, producing a $Ti^{III}-N_2^{2-}-Ti^{III}$ core. A combination of electrochemical, reactivity, spectroscopic, and structural studies demonstrate that THF coordinates reversibly to **2** with a fairly high association constant on the order of 5−8 M^{-1}; the so-formed **2-THF** adduct is impervious to N_2 binding, implying the intermediacy of a four-coordinate geometry in reactions, where **1** is reduced to generate **2** as well as **3**. Even when using a strong-field ligand, such as CNAd, complex **2** forms a five-coordinate adduct, **2-CNAd**, while preserving the high-spin nature of the Ti^{II} ion, owing to only a moderate degree of π-back-bonding, as seen from the linear Ti−C−N geometry [174.2(1)°] and slight redshift of ν(C≡N) (28 cm^{-1}). The availability of an open coordination site as well as two energetically high-lying d electrons renders tetrahedral **2** a versatile precursor to a family of five-coordinate Ti^{IV} complexes of the type $[(Tp^{tBu,Me})Ti{\equiv}E(Cl)]$, with E^{2-} = O, NH, $NSiMe_3$, and N_2CPh_2. These products result from O-atom transfer from N_2O and NH group transfer from the bicyclic amine Hdbabh to generate respectively the corresponding terminal oxide and parent terminal imide complexes. While N_3SiMe_3 reacts with **2** under N_2 extrusion, N_2CPh_2 retains an intact N=N=C spine up to 100 °C.

We are presently scrutinizing the unique electronic structure of additional tetrahedral Ti^{II} complexes, as well as examining their potential for generating unusual metal−ligand multiple bonds.

■ ASSOCIATED CONTENT

Supporting Information

The Supporting Information is available free of charge at https://pubs.acs.org/doi/10.1021/acs.inorgchem.0c02586.

NMR, XRD, cyclic voltammetry, SQUID, X- and Q-band EPR, HFEPR, Ti K-edge XAS, and computational data (PDF)

Accession Codes

CCDC 2005728−2005738 contain the supplementary crystallographic data for this paper. These data can be obtained free of charge *via* www.ccdc.cam.ac.uk/data_request/cif, or by emailing data_request@ccdc.cam.ac.uk, or by contacting The Cambridge Crystallographic Data Centre, 12 Union Road, Cambridge CB2 1EZ, UK; fax: +44 1223 336033.

■ AUTHOR INFORMATION

Corresponding Authors

Joshua Telser − *Department of Biological, Physical and Health Sciences, Roosevelt University, Chicago, Illinois 60605, United States;* orcid.org/0000-0003-3307-2556; Email: jtelser@roosevelt.edu

Kyle M. Lancaster − *Baker Laboratory, Department of Chemistry and Chemical Biology, Cornell University, Ithaca, New York 14853, United States;* orcid.org/0000-0001-7296-128X; Email: kml236@cornell.edu

Karsten Meyer − *Inorganic Chemistry, Department of Chemistry and Pharmacy, Friedrich-Alexander University (FAU) Erlangen-Nürnberg, 91058 Erlangen, Germany;* orcid.org/0000-0002-7844-2998; Email: karsten.meyer@fau.de

Daniel J. Mindiola − *Department of Chemistry, University of Pennsylvania, Philadelphia, Pennsylvania 19104, United States;* orcid.org/0000-0001-8205-7868; Email: mindiola@sas.upenn.edu

Authors

Anders Reinholdt − *Department of Chemistry, University of Pennsylvania, Philadelphia, Pennsylvania 19104, United States;* orcid.org/0000-0001-6637-8338

Daniel Pividori − *Inorganic Chemistry, Department of Chemistry and Pharmacy, Friedrich-Alexander University (FAU) Erlangen-Nürnberg, 91058 Erlangen, Germany*

Alexander L. Laughlin − *Baker Laboratory, Department of Chemistry and Chemical Biology, Cornell University, Ithaca, New York 14853, United States*

Ida M. DiMucci − *Baker Laboratory, Department of Chemistry and Chemical Biology, Cornell University, Ithaca, New York 14853, United States;* orcid.org/0000-0003-3440-7856

Samantha N. MacMillan − *Baker Laboratory, Department of Chemistry and Chemical Biology, Cornell University, Ithaca, New York 14853, United States;* orcid.org/0000-0001-6516-1823

Mehrafshan G. Jafari − *Department of Chemistry, University of Pennsylvania, Philadelphia, Pennsylvania 19104, United States;* orcid.org/0000-0001-6807-7520

Michael R. Gau − *Department of Chemistry, University of Pennsylvania, Philadelphia, Pennsylvania 19104, United States;* orcid.org/0000-0002-4790-6980

Patrick J. Carroll − *Department of Chemistry, University of Pennsylvania, Philadelphia, Pennsylvania 19104, United States*

J. Krzystek − *National High Magnetic Field Laboratory, Florida State University, Tallahassee, Florida 32310, United States;* orcid.org/0000-0001-6088-1936

https://dx.doi.org/10.1021/acs.inorgchem.0c02586
Inorg. Chem. 2020, 59, 17834−17850

Andrew Ozarowski − *National High Magnetic Field Laboratory, Florida State University, Tallahassee, Florida 32310, United States;* orcid.org/0000-0001-6225-9796

Complete contact information is available at: https://pubs.acs.org/10.1021/acs.inorgchem.0c02586

Author Contributions

The manuscript was written through contributions of all authors. All authors have given approval to the final version of the manuscript.

Notes

The authors declare no competing financial interest.

■ ACKNOWLEDGMENTS

A.R. gratefully acknowledges The Carlsberg Foundation (Grant CF18-0613) and the Independent Research Fund Denmark (Grant 9036-00015B) for funding. We thank the U.S. National Science Foundation (NSF; Grants CHE-0848248 and CHE-1152123 to D.J.M. and Grant CHE-1454455 to K.M.L.) and the University of Pennsylvania for financial support of this research. Part of this work was performed at the National High Magnetic Field Laboratory, which is supported by NSF Cooperative Agreement DMR-1644779 and the State of Florida. EPR studies at Northwestern University were supported by the U.S. Department of Energy (DOE), Office of Science, Basic Energy Sciences, under Contract DE-SC0019342 (to Prof. Brian M. Hoffman). XAS data were obtained at Stanford Synchrotron Radiation Lightsource (SSRL), which is supported by the U.S. DOE, Office of Science, Office of Basic Energy Sciences, under Contract DE-AC02-76SF00515. The SSRL Structural Molecular Biology Program is supported by the U.S. DOE, Office of Biological and Environmental Research, and by National Institutes of Health (NIH)/National Institute of General Medical Sciences (including P41GM103393). The authors also acknowledge the NIH Supplemental Awards 3R01GM118510-03S1 and 3R01GM087605-06S1 and financial support of the Vagelos Institute for Energy Sciences and Technology for the purchase of NMR instrument NEO600. K.M. acknowledges generous funding from FAU Erlangen-Nürnberg.

■ REFERENCES

(1) (a) McMurry, J. E. Carbonyl-coupling reactions using low-valent titanium. *Chem. Rev.* **1989**, *89*, 1513−1524. (b) Kulinkovich, O. G.; Sviridov, S. V.; Vasilevski, D. A. Titanium(IV) Isopropoxide-Catalyzed Formation of 1-Substituted Cyclopropanols in the Reaction of Ethylmagnesium Bromide with Methyl Alkanecarboxylates. *Synthesis* **1991**, *1991*, 234−234. (c) Aleandri, L. E.; Bogdanović, B.; Gaidies, A.; Jones, D. J.; Liao, S.; Michalowicz, A.; Rozière, J.; Schott, A. $[Ti(MgCl)_2 \cdot xTHF]_q$: a reagent for the McMurry reaction and a novel inorganic Grignard complex. *J. Organomet. Chem.* **1993**, *459*, 87−93. (d) Fürstner, A. Chemistry of and with Highly Reactive Metals. *Angew. Chem. Angew. Chem., Int. Ed. Engl.* **1993**, *32*, 164−189. (e) Kulinkovich, O. G.; de Meijere, A. 1,*n*-Dicarbanionic Titanium Intermediates from Monocarbanionic Organometallics and Their Application in Organic Synthesis. *Chem. Rev.* **2000**, *100*, 2789−2834.

(2) (a) Gilbert, Z. W.; Hue, R. J.; Tonks, I. A. Catalytic formal [2 + 2+1] synthesis of pyrroles from alkynes and diazenes via Ti^{II}/Ti^{IV} redox catalysis. *Nat. Chem.* **2016**, *8*, 63−68. (b) Davis-Gilbert, Z. W.; Yao, L. J.; Tonks, I. A. Ti-Catalyzed Multicomponent Oxidative Carboamination of Alkynes with Alkenes and Diazenes. *J. Am. Chem. Soc.* **2016**, *138*, 14570−14573. (c) Chiu, H.-C.; Tonks, I. A. Trimethylsilyl-Protected Alkynes as Selective Cross-Coupling Partners in Titanium-Catalyzed [2 + 2+1] Pyrrole Synthesis. *Angew. Chem., Int. Ed.* **2018**, *57*, 6090−6094. (d) Davis-Gilbert, Z. W.; Wen, X.; Goodpaster, J. D.; Tonks, I. A. Mechanism of Ti-Catalyzed Oxidative Nitrene Transfer in [2 + 2 + 1] Pyrrole Synthesis from Alkynes and Azobenzene. *J. Am. Chem. Soc.* **2018**, *140*, 7267−7281. (e) Pearce, A. J.; See, X. Y.; Tonks, I. A. Oxidative nitrene transfer from azides to alkynes *via* Ti(II)/Ti(IV) redox catalysis: formal [2 + 2+1] synthesis of pyrroles. *Chem. Commun.* **2018**, *54*, 6891−6894. (f) Beaumier, E. P.; McGreal, M. E.; Pancoast, A. R.; Wilson, R. H.; Moore, J. T.; Graziano, B. J.; Goodpaster, J. D.; Tonks, I. A. Carbodiimide Synthesis via Ti-Catalyzed Nitrene Transfer from Diazenes to Isocyanides. *ACS Catal.* **2019**, *9*, 11753−11762. (g) Chiu, H.-C.; See, X. Y.; Tonks, I. A. Dative Directing Group Effects in Ti-Catalyzed [2 + 2+1] Pyrrole Synthesis: Chemo- and Regioselective Alkyne Heterocoupling. *ACS Catal.* **2019**, *9*, 216−223. (h) Reiner, B. R.; Tonks, I. A. Group 4 Diarylmetallocenes as Bespoke Aryne Precursors for Titanium-Catalyzed [2 + 2 + 2] Cycloaddition of Arynes and Alkynes. *Inorg. Chem.* **2019**, *58*, 10508−10515. (i) Beaumier, E. P.; Gordon, C. P.; Harkins, R. P.; McGreal, M. E.; Wen, X.; Copéret, C.; Goodpaster, J. D.; Tonks, I. A. $Cp_2Ti(\kappa^2\text{-}^t\text{BuNCN}^t\text{Bu})$: A Complex with an Unusual κ^2 Coordination Mode of a Heterocumulene Featuring a Free Carbene. *J. Am. Chem. Soc.* **2020**, *142*, 8006−8018. (j) Pearce, A. J.; Harkins, R. P.; Reiner, B. R.; Wotal, A. C.; Dunscomb, R. J.; Tonks, I. A. Multicomponent Pyrazole Synthesis from Alkynes, Nitriles, and Titanium Imido Complexes *via* Oxidatively Induced N−N Bond Coupling. *J. Am. Chem. Soc.* **2020**, *142*, 4390−4399. (k) Beaumier, E. P.; Ott, A. A.; Wen, X.; Davis-Gilbert, Z. W.; Wheeler, T. A.; Topczewski, J. J.; Goodpaster, J. D.; Tonks, I. A. Ti-catalyzed ring-opening oxidative amination of methylenecyclopropanes with diazenes. *Chem. Sci.* **2020**, *11*, 7204.

(3) (a) Girolami, G. S.; Wilkinson, G.; Galas, A. M. R.; Thornton-Pett, M.; Hursthouse, M. B. Synthesis and Properties of the Divalent 1,2-Bis(dimethylphosphino)ethane (dmpe) Complexes $MCl_2(dmpe)_2$ and $MMe_2(dmpe)_2$ (M = Ti, V, Cr, Mn, or Fe). *X*-Ray Crystal Structures of $MCl_2(dmpe)_2$ (M = Ti, V, or Cr), $MnBr_2(dmpe)_2$, $TiMe_{1.3}Cl_{0.7}(dmpe)_2$, and $CrMe_2(dmpe)_2$. *J. Chem. Soc., Dalton Trans.* **1985**, 1339−1348. (b) Jensen, J. A.; Wilson, S. R.; Schultz, A. J.; Girolami, G. S. Divalent Titanium Chemistry. Synthesis, Reactivity, and X-ray and Neutron Diffraction Studies of $Ti(BH_4)_2(dmpe)_2$ and $Ti(CH_3)_2(dmpe)_2$. *J. Am. Chem. Soc.* **1987**, *109*, 8094−8096. (c) Jensen, J. A.; Girolami, G. S. Synthesis, Characterization, and X-ray Crystal Structures of the Divalent Titanium Complex $Ti(\eta^2\text{-}BH_4)_2(dmpe)_2$ and the unidentate tetrahydroborate complex $V(\eta^1\text{-}BH_4)_2(dmpe)_2$. *Inorg. Chem.* **1989**, *28*, 2107−2113. (d) Morris, R. J.; Girolami, G. S. On the π-Donor Ability of Early Transition Metals: Evidence That Trialkylphosphines Can Engage in π-Back-Bonding and X-ray Structure of the Titanium(II) Phenoxide $Ti(OPh)_2(dmpe)_2$. *Inorg. Chem.* **1990**, *29*, 4167−4169.

(4) (a) Edema, J. J. H.; Duchateau, R.; Gambarotta, S.; Hynes, R.; Gabe, E. Novel Titanium(II) Amine Complexes L_4TiCl_2 [L = $^1/_2$ *N,N,N′,N′*-tetramethylethylenediamine (TMEDA), $^1/_2$ *N,N,N′*-trimethylethylenediamine, pyridine, $^1/_2$ 2,2′-bipyridine]: Synthesis and Crystal Structure of Monomeric *trans*-$(TMEDA)_2TiCl_2$. *Inorg. Chem.* **1991**, *30*, 154−156. (b) Zolnhofer, E. M.; Wijeratne, G. B.; Jackson, T. A.; Fortier, S.; Heinemann, F. W.; Meyer, K.; Krzystek, J.; Ozarowski, A.; Mindiola, D. J.; Telser, J. Electronic Structure and Magnetic Properties of a Titanium(II) Coordination Complex. *Inorg. Chem.* **2020**, *59*, 6187−6201. (c) Araya, M. A.; Cotton, F. A.; Matonic, J. H.; Murillo, C. A. An Efficient Reduction Process Leading to Titanium(II) and Niobium(II): Preparation and Structural Characterization of *trans*-$MCl_2(py)_4$ Compounds, M = Ti, Nb, and Mn. *Inorg. Chem.* **1995**, *34*, 5424−5428. (d) Wijeratne, G. B.; Zolnhofer, E. M.; Fortier, S.; Grant, L. N.; Carroll, P. J.; Chen, C.-H.; Meyer, K.; Krzystek, J.; Ozarowski, A.; Jackson, T. A.; Mindiola, D. J.; Telser, J. Electronic Structure and Reactivity of a Well-Defined Mononuclear Complex of Ti(II). *Inorg. Chem.* **2015**, *54*, 10380−10397.

(5) (a) Woo, L. K.; Hays, J. A.; Young, V. G.; Day, C. L.; Caron, C.; D'Souza, F.; Kadish, K. M. Synthesis, Characterization, Substitution, and Atom-Transfer Reactions of (η^2-Alkyne)(tetratolylporphyrinato)-

titanium(II). X-ray Structure of *trans*-Bis(4-picoline)-(tetratolylporphyrinato)titanium(II). *Inorg. Chem.* **1993**, *32*, 4186−4192. (b) Thorman, J. L.; Young, V. G.; Boyd, P. D. W.; Guzei, I. A.; Woo, L. K. Atom Transfer Reactions of (TTP)Ti(η^2-3-hexyne): Synthesis and Molecular Structure of *trans*-(TTP)Ti[OP(Oct)$_3$]$_2$. *Inorg. Chem.* **2001**, *40*, 499−506. (c) Wang, X.; Gray, S. D.; Chen, J.; Woo, L. K. Facile Syntheses of Titanium(II), Tin(II), and Vanadium(II) Porphyrin Complexes through Homogeneous Reduction. Reactivity of *trans*-(TTP)TiL$_2$ (L = THF, *t*-BuNC). *Inorg. Chem.* **1998**, *37*, 5−9.

(6) Kayal, A.; Kuncheria, J.; Lee, S. C. Bis[hydrotris(pyrazol-1-yl)borato]titanium(II): a stable Tp$_2$M complex of singular reactivity. *Chem. Commun.* **2001**, 2482−2483.

(7) (a) Hagadorn, J. R.; Arnold, J. Low-Valent Chemistry of Titanium Benzamidinates Leading to New Ti μ-N$_2$, μ-O, Alkyl Derivatives, and the Cyclometalation of TMEDA. *J. Am. Chem. Soc.* **1996**, *118*, 893−894. (b) Hagadorn, J. R.; Arnold, J. Titanium(II), -(III), and -(IV) Complexes Supported by Benzamidinate Ligands. *Organometallics* **1998**, *17*, 1355−1368. (c) Baumann, R.; Stumpf, R.; Davis, W. M.; Liang, L.-C.; Schrock, R. R. Titanium and Zirconium Complexes That Contain the Tridentate Diamido Ligands [(*i*-PrN-*o*-C$_6$H$_4$)$_2$O]$^{2-}$ ([*i*-PrNON]$^{2-}$) and [(C$_6$H$_{11}$N-*o*-C$_6$H$_4$)$_2$O]$^{2-}$ ([CyNON]$^{2-}$). *J. Am. Chem. Soc.* **1999**, *121*, 7822−7836. (d) Bai, G.; Wei, P.; Stephan, D. W. Reductions of β-Diketiminato−Titanium(III) Complexes. *Organometallics* **2006**, *25*, 2649−2655. (e) Chomitz, W. A.; Arnold, J. Transition metal dinitrogen complexes supported by a versatile monoanionic [N$_2$P$_2$] ligand. *Chem. Commun.* **2007**, 4797−4799. (f) Hanna, T. E.; Bernskoetter, W. H.; Bouwkamp, M. W.; Lobkovsky, E.; Chirik, P. J. Bis(cyclopentadienyl) Titanium Dinitrogen Chemistry: Synthesis and Characterization of a Side-on Bound Haptomer. *Organometallics* **2007**, *26*, 2431−2438. (g) Semproni, S. P.; Milsmann, C.; Chirik, P. J. Side-on Dinitrogen Complexes of Titanocenes with Disubstituted Cyclopentadienyl Ligands: Synthesis, Structure, and Spectroscopic Characterization. *Organometallics* **2012**, *31*, 3672−3682. (h) Kurogi, T.; Ishida, Y.; Kawaguchi, H. Synthesis of titanium and zirconium complexes supported by a *p*-terphenoxide ligand and their reactions with N$_2$, CO$_2$ and CS$_2$. *Chem. Commun.* **2013**, *49*, 11755−11757. (i) Doyle, L. R.; Wooles, A. J.; Jenkins, L. C.; Tuna, F.; McInnes, E. J. L.; Liddle, S. T. Catalytic Dinitrogen Reduction to Ammonia at a Triamidoamine−Titanium Complex. *Angew. Chem., Int. Ed.* **2018**, *57*, 6314−6318. (j) Sekiguchi, Y.; Meng, F.; Tanaka, H.; Eizawa, A.; Arashiba, K.; Nakajima, K.; Yoshizawa, K.; Nishibayashi, Y. Synthesis and reactivity of titanium- and zirconium-dinitrogen complexes bearing anionic pyrrole-based PNP-type pincer ligands. *Dalton Trans.* **2018**, *47*, 11322−11326. (k) Ghana, P.; van Krüchten, F. D.; Spaniol, T. P.; van Leusen, J.; Kögerler, P.; Okuda, J. Conversion of dinitrogen to tris-(trimethylsilyl)amine catalyzed by titanium triamido-amine complexes. *Chem. Commun.* **2019**, *55*, 3231−3234. (l) Nakanishi, Y.; Ishida, Y.; Kawaguchi, H. Nitrogen−Carbon Bond Formation by Reactions of a Titanium−Potassium Dinitrogen Complex with Carbon Dioxide, *tert*-Butyl Isocyanate, and Phenylallene. *Angew. Chem., Int. Ed.* **2017**, *56*, 9193−9197.

(8) (a) Atwood, J. L.; Stone, K. E.; Alt, H. G.; Hrncir, D. C.; Rausch, M. D. The crystal structure of dicarbonyldicyclopentadienyltitanium-(II), (η^5-C$_5$H$_5$)$_2$Ti(CO)$_2$. *J. Organomet. Chem.* **1977**, *132*, 367−375. (b) Hollis, T. K.; Ahn, Y. J.; Tham, F. S. Low-Valent Titanium Bis(phospholyl) Chemistry: A Configurationally Stable Chiral Phosphatitanocene. *Organometallics* **2003**, *22*, 1432−1436. (c) Hanna, T. E.; Lobkovsky, E.; Chirik, P. J. Mono(dinitrogen) and Carbon Monoxide Adducts of Bis(cyclopentadienyl) Titanium Sandwiches. *J. Am. Chem. Soc.* **2006**, *128*, 6018−6019. (d) Kilpatrick, A. F. R.; Cloke, F. G. N. Reductive deoxygenation of CO$_2$ by a bimetallic titanium bis(pentalene) complex. *Chem. Commun.* **2014**, *50*, 2769−2771. (e) Aguilar-Calderón, J. R.; Metta-Magaña, A. J.; Noll, B.; Fortier, S. C(sp^3)−H Oxidative Addition and Transfer Hydrogenation Chemistry of a Titanium(II) Synthon: Mimicry of Late-Metal Type Reactivity. *Angew. Chem., Int. Ed.* **2016**, *55*, 14101−14105.

(9) (a) Kool, L. B.; Rausch, M. D.; Herberhold, M.; Alt, H. G.; Thewalt, U.; Honold, B. Diamagnetic isocyanide complexes of titanium, zirconium, and hafnium. *Organometallics* **1986**, *5*, 2465−2468. (b) Cuenca, T.; Gómez, R.; Gomez-Sal, P.; Royo, P. Synthesis and characterization of ansa-dimethylsilylbiscyclopentadienyl titanium(II) complexes. Crystal structure of [Ti{Me$_2$Si(C$_5$H$_4$)$_2$}{CN-(2,6-Me$_2$C$_6$H$_3$)}$_2$]. *J. Organomet. Chem.* **1993**, *454*, 105−111. (c) Haehnel, M.; Ruhmann, M.; Theilmann, O.; Roy, S.; Beweries, T.; Arndt, P.; Spannenberg, A.; Villinger, A.; Jemmis, E. D.; Schulz, A.; Rosenthal, U. Reactions of Titanocene Bis(trimethylsilyl)acetylene Complexes with Carbodiimides: An Experimental and Theoretical Study of Complexation versus C−N Bond Activation. *J. Am. Chem. Soc.* **2012**, *134*, 15979−15991. (d) Altenburger, K.; Arndt, P.; Becker, L.; Reiß, F.; Burlakov, V. V.; Spannenberg, A.; Baumann, W.; Rosenthal, U. Multiple and Highly Selective Alkyne−Isonitrile C−C and C−N Couplings at Group 4 Metallocenes. *Chem. - Eur. J.* **2016**, *22*, 9169−9180.

(10) (a) McPherson, A. M.; Fieselmann, B. F.; Lichtenberger, D. L.; McPherson, G. L.; Stucky, G. D. Electronic Properties of Bis(η^5-cyclopentadienyl)titanium 2,2′-Bipyridyl. A Singlet Molecule with a Low-Lying Triplet Excited State. *J. Am. Chem. Soc.* **1979**, *101*, 3425−3430. (b) Durfee, L. D.; Fanwick, P. E.; Rothwell, I. P.; Folting, K.; Huffman, J. C. Reductive Elimination Pathways to Low Valent Titanium Aryl Oxide Complexes. *J. Am. Chem. Soc.* **1987**, *109*, 4720−4722. (c) Piglosiewicz, I. M.; Beckhaus, R.; Saak, W.; Haase, D. Dehydroaromatization of Quinoxalines: One-Step Syntheses of Trinuclear 1,6,7,12,13,18-Hexaazatrinaphthylene Titanium Complexes. *J. Am. Chem. Soc.* **2005**, *127*, 14190−14191.

(11) (a) Corbin, D. R.; Willis, W. S.; Duesler, E. N.; Stucky, G. D. Intramolecular Electron-Transfer Induced Carbon-Hydrogen Bond Dissociation in Methyl-Substituted 1,10-Phenanthroline Complexes of Bis(η^5-cyclopentadienyl)titanium. *J. Am. Chem. Soc.* **1980**, *102*, 5969−5971. (b) Wolff, C.; Gottschlich, A.; England, J.; Wieghardt, K.; Saak, W.; Haase, D.; Beckhaus, R. , Molecular and Electronic Structures of Mononuclear and Dinuclear Titanium Complexes Containing π-Radical Anions of 2,2′-Bipyridine and 1,10-Phenanthroline: An Experimental and DFT Computational Study. *Inorg. Chem.* **2015**, *54*, 4811−4820.

(12) (a) Schmid, G.; Thewalt, U.; Polášek, M.; Mach, K.; Sedmera, P. η^5-Pentabenzylcyclopentadienyl derivatives of titanium (IV), (III), and (II). The crystal structures of (η^5-C$_5$H$_5$)(η^5-C$_5$Bz$_5$)TiCl$_2$ (Bz = benzyl), (η^5-C$_5$H$_5$)(η^5- C$_5$Bz$_5$)TiCl, and (η^5-C$_5$H$_5$)(η^5-C$_5$Bz$_5$)Ti[η^2-(CSiMe$_3$)$_2$]. *J. Organomet. Chem.* **1994**, *482*, 231−241. (b) Noor, A.; Kempe, R. Acetylenetitanium Complex Stabilized by Aminopyridinato Ligands. *Eur. J. Inorg. Chem.* **2008**, *2008*, 2377−2381. (c) Lamač, M.; Spannenberg, A.; Baumann, W.; Jiao, H.; Fischer, C.; Hansen, S.; Arndt, P.; Rosenthal, U. Si−H Bond Activation of Alkynylsilanes by Group 4 Metallocene Complexes. *J. Am. Chem. Soc.* **2010**, *132*, 4369−4380. (d) Haehnel, M.; Hansen, S.; Schubert, K.; Arndt, P.; Spannenberg, A.; Jiao, H.; Rosenthal, U. Synthesis, Characterization and Reactivity of Group 4 Metallocene Bis(diphenylphosphino)-acetylene Complexes—A Reactivity and Bonding Study. *J. Am. Chem. Soc.* **2013**, *135*, 17556−17565. (e) Pinkas, J.; Gyepes, R.; Císařová, I.; Kubišta, J.; Horáček, M.; Mach, K. Displacement of ethene from the decamethyltitanocene-ethene complex with internal alkynes, substituent-dependent alkyne-to-allene rearrangement, and the electronic transition relevant to the back-bonding interaction. *Dalton Trans.* **2015**, *44*, 7276−7291.

(13) (a) Cohen, S. A.; Auburn, P. R.; Bercaw, J. E. Structure and reactivity of bis(pentamethylcyclopentadienyl)(ethylene)titanium(II), a simple olefin adduct of titanium. *J. Am. Chem. Soc.* **1983**, *105*, 1136−1143. (b) Horáček, M.; Kupfer, V.; Thewalt, U.; Štěpnička, P.; Polášek, M.; Mach, K. Bis[η^5-tetramethyl(trimethylsilyl)-cyclopentadienyl]titanium(II) and Its π-Complexes with Bis-(trimethylsilyl)acetylene and Ethylene. *Organometallics* **1999**, *18*, 3572−3578. (c) Pinkas, J.; Císařová, I.; Gyepes, R.; Kubišta, J.; Horáček, M.; Mach, K. Ethene Complexes of Bulky Titanocenes, Their Thermolysis, and Their Reactivity toward 2-Butyne. *Organometallics* **2012**, *31*, 5478−5493.

https://dx.doi.org/10.1021/acs.inorgchem.0c02586
Inorg. Chem. 2020, 59, 17834−17850

(14) (a) Breil, H.; Wilke, G. Di(cyclooctatetraene)titanium and Tri(cyclooctatetraene)dititanium. *Angew. Chem., Int. Ed. Engl.* **1966**, *5*, 898−899. (b) Dietrich, H.; Soltwisch, M. Crystal Structure of Bis(cyclooctatetraene)titanium. *Angew. Chem., Int. Ed. Engl.* **1969**, *8*, 765−765. (c) Cloke, F. G. N.; Green, J. C.; Hitchcock, P. B.; Joseph, S. C. P.; Mountford, P.; Kaltsoyannis, N.; McCamley, A. Molecular and electronic structures of bis[1,4-bis(trimethylsilyl)-cyclooctatetraene] sandwich complexes of titanium and zirconium. *J. Chem. Soc., Dalton Trans.* **1994**, 2867−2874. (d) Horáček, M.; Hiller, J.; Thewalt, U.; Štěpnička, P.; Mach, K. Bis[(η^8-cyclooctatetraene)titanium] complex with perpendicularly bridging bis(trimethylsilyl)acetylene. *J. Organomet. Chem.* **1998**, *571*, 77−82.

(15) (a) Sikora, D. J.; Rausch, M. D.; Rogers, R. D.; Atwood, J. L. Formation and Molecular Structure of Bis(η^5-cyclopentadienyl)bis-(trifluorophosphine)titanium. *J. Am. Chem. Soc.* **1981**, *103*, 982−984. (b) Arp, H.; Baumgartner, J.; Marschner, C.; Zark, P.; Müller, T. Coordination Chemistry of Cyclic Disilylated Stannylenes and Plumbylenes to Group 4 Metallocenes. *J. Am. Chem. Soc.* **2012**, *134*, 10864−10875.

(16) (a) Hitchcock, P. B.; Kerton, F. M.; Lawless, G. A. The Elusive Titanocene. *J. Am. Chem. Soc.* **1998**, *120*, 10264−10265. (b) Kilpatrick, A. F. R.; Green, J. C.; Cloke, F. G. N.; Tsoureas, N. Bis(pentalene)di-titanium: a bent double-sandwich complex with a very short Ti−Ti bond. *Chem. Commun.* **2013**, *49*, 9434−9436.

(17) Edema, J. J. H.; Gambarotta, S.; Duchateau, R.; Bensimon, C. Labile triangulo-trititanium(II) and trivanadium(II) clusters. *Inorg. Chem.* **1991**, *30*, 3585−3587.

(18) Ma, W.; Zhang, J.-X.; Lin, Z.; Tilley, T. D.; Ye, Q. Synthesis, structure and DFT calculations of mononuclear cyclic (alkyl)(amino) carbene supported titanium(II) complexes. *Dalton Trans.* **2019**, *48*, 14962−14965.

(19) Liu, Q.; Chen, Q.; Leng, X.; Deng, Q.-H.; Deng, L. Hafnium(II) Complexes with Cyclic (Alkyl)(amino)carbene Ligation. *Organometallics* **2018**, *37*, 4186−4188.

(20) (a) Trofimenko, S. Coordination chemistry of pyrazole-derived ligands. *Chem. Rev.* **1972**, *72*, 497−509. (b) Trofimenko, S. Recent Advances in Poly(pyrazolyl)borate (Scorpionate) Chemistry. *Chem. Rev.* **1993**, *93*, 943−980.

(21) Dowling, C. M.; Leslie, D.; Chisholm, M. H.; Parkin, G. The Synthesis and Structural Characterization of the Sterically Demanding Tris(3,5-di-t-butylpyrazolyl)hydroborato Ligand, [Tp^{But2}]: A Highly Twisted, Propeller-Like, Ligand System. *Main Group Chem.* **1995**, *1*, 29−52.

(22) Petrov, P. A.; Smolentsev, A. I.; Bogomyakov, A. S.; Konchenko, S. N. Novel vanadium complexes supported by a bulky tris(pyrazolyl)borate ligand. *Polyhedron* **2017**, *129*, 60−64.

(23) Kersten, J. L.; Kucharczyk, R. R.; Yap, G. P. A.; Rheingold, A. L.; Theopold, K. H. [($Tp^{tBu,Me}$)CrR]: A New Class of Mononuclear, Coordinatively Unsaturated Chromium(II) Alkyls with *cis*-Divacant Octahedral Structure. *Chem. - Eur. J.* **1997**, *3*, 1668−1674.

(24) (a) Brunker, T. J.; Hascall, T.; Cowley, A. R.; Rees, L. H.; O'Hare, D. Variable Coordination Modes of Hydrotris(3-isopropyl-4-bromopyrazolyl)borate (Tp′) in Fe(II), Mn(II), Cr(II), and Cr(III) Complexes: Formation of MTp′Cl (M = Fe and Mn), Structural Isomerism in $CrTp'_2$, and the Observation of Tp'^- as an Uncoordinated Anion. *Inorg. Chem.* **2001**, *40*, 3170−3176. (b) Nabika, M.; Seki, Y.; Miyatake, T.; Ishikawa, Y.; Okamoto, K.-i.; Fujisawa, K. Manganese Catalysts with Scorpionate Ligands for Olefin Polymerization. *Organometallics* **2004**, *23*, 4335−4337. (c) Tietz, T.; Limberg, C.; Stößer, R.; Ziemer, B. Four-Coordinate Trispyrazolylborato-manganese and -iron Complexes with a Pyrazolato Co-ligand: Syntheses and Properties as Oxidation Catalysts. *Chem. - Eur. J.* **2011**, *17*, 10010−10020. (d) Gorrell, I. B.; Parkin, G. (Tris-(3-*tert*-butylpyrazolyl)hydroborato)manganese(II), -iron(II), -cobalt(II), and -nickel(II) Halide Derivatives: Facile Abstraction of Fluoride from $[BF_4]^-$. *Inorg. Chem.* **1990**, *29*, 2452−2456.

(25) (a) Jové, F. A.; Pariya, C.; Scoblete, M.; Yap, G. P. A.; Theopold, K. H. A Family of Four-Coordinate Iron(II) Complexes Bearing the Sterically Hindered Tris(pyrazolyl)borato Ligand $Tp^{tBu,Me}$. *Chem. - Eur. J.* **2011**, *17*, 1310−1318. (b) Fujisawa, K.; Soma, S.; Kurihara, H.; Ohta, A.; Dong, H. T.; Minakawa, Y.; Zhao, J.; Alp, E. E.; Hu, M. Y.; Lehnert, N. Stable Ferrous Mononitroxyl $\{FeNO\}^8$ Complex with a Hindered Hydrotris(pyrazolyl)borate Coligand: Structure, Spectroscopic Characterization, and Reactivity Toward NO and O_2. *Inorg. Chem.* **2019**, *58*, 4059−4062.

(26) (a) Uehara, K.; Hikichi, S.; Akita, M. Highly labile cationic tris-acetonitrile complexes, [$Tp^RM(NCMe)_3$]OTf (M = Ni, Co; Tp^R: hydrotrispyrazolylborato, R = Ph, Me and iPr_2): versatile precursors for Tp^R-containing nickel and cobalt complexes. *J. Chem. Soc., Dalton Trans.* **2002**, 3529−3538. (b) Rheingold, A. L.; Liable-Sands, L. M.; Golan, J. A.; Trofimenko, S. Remote Rotamer Control: The Effect of a 4-*tert*-Butyl Group on the Coordination Chemistry of Tp^R Ligands. *Eur. J. Inorg. Chem.* **2003**, *2003*, 2767−2773. (c) Rheingold, A. L.; Liable-Sands, L. M.; Golen, J. A.; Yap, G. P. A.; Trofimenko, S. The coordination chemistry of the hydrotris(3-diphenylmethylpyrazol-1-yl)borate (Tp^{CHPh2}) ligand. *Dalton Trans.* **2004**, 598−604. (d) Trofimenko, S.; Rheingold, A. L.; Liable Sands, L. M. Coordination Chemistry of Novel Scorpionate Ligands Based on 3-Cyclohexylpyrazole and 3-Cyclohexyl-4-bromopyrazole. *Inorg. Chem.* **2002**, *41*, 1889−1896. (e) Krzystek, J.; Swenson, D. C.; Zvyagin, S. A.; Smirnov, D.; Ozarowski, A.; Telser, J. Cobalt(II) "Scorpionate" Complexes as Models for Cobalt-Substituted Zinc Enzymes: Electronic Structure Investigation by High-Frequency and -Field Electron Paramagnetic Resonance Spectroscopy. *J. Am. Chem. Soc.* **2010**, *132*, 5241−5253.

(27) (a) Guo, S.; Ding, E.; Yin, Y.; Yu, K. Synthesis and structures of tris(pyrazolyl)hydroborato metal complexes as structural model compounds of carbonicanhydrase. *Polyhedron* **1998**, *17*, 3841−3849. (b) Belderraín, T. R.; Paneque, M.; Carmona, E.; Gutiérrez-Puebla, E.; Monge, M. A.; Ruiz-Valero, C. Three-Center, Two-Electron M···H−B Bonds in Complexes of Ni, Co, and Fe and the Dihydrobis(3-*tert*-butylpyrazolyl)borate Ligand. *Inorg. Chem.* **2002**, *41*, 425−428. (c) Kunrath, F. A.; de Souza, R. F.; Casagrande, O. L.; Brooks, N. R.; Young, V. G. Highly Selective Nickel Ethylene Oligomerization Catalysts Based on Sterically Hindered Tris(pyrazolyl)borate Ligands. *Organometallics* **2003**, *22*, 4739−4743. (d) Frampton, A. K.; Gartland, K.; Piro, N. A.; Kassel, W. S.; Dougherty, W. G. Structural characterization and electrochemical properties of nickel (II) complexes bearing sterically bulky hydrotris(3-phenyl)- and hydrotris-(3-*tert*-butylpyrazol-1-yl)borato ligands. *Polyhedron* **2016**, *114*, 172−178.

(28) (a) Kitajima, N.; Fujisawa, K.; Morooka, Y. Tetrahedral copper(II) complexes supported by a hindered pyrazolylborate. Formation of the thiolato complex, which closely mimics the spectroscopic characteristics of blue copper proteins. *J. Am. Chem. Soc.* **1990**, *112*, 3210−3212. (b) Yoon, K.; Parkin, G. Tris(3-t-butyl-5-methylpyrazolyl)hydroborato derivatives of copper and thallium: The structural influence of a 5-methyl substituent. *Polyhedron* **1995**, *14*, 811−821. (c) Higashimura, H.; Kubota, M.; Shiga, A.; Fujisawa, K.; Moro-oka, Y.; Uyama, H.; Kobayashi, S. Radical-Controlled" Oxidative Polymerization of 4-Phenoxyphenol by a Tyrosinase Model Complex Catalyst to Poly(1,4-phenylene oxide). *Macromolecules* **2000**, *33*, 1986−1995. (d) Fujisawa, K.; Tada, N.; Ishikawa, Y.; Higashimura, H.; Miyashita, Y.; Okamoto, K.-i. The most hindered hydrotris(pyrazolyl)borate ligand, X-ray structure of chlorocopper(II) complex: [Cu(Cl){HB(3-Ad-5-Pr^ipz)$_3$}] as compared with [Cu(Cl){HB(3-Bu^t-5-Pr^ipz)$_3$}]. *Inorg. Chem. Commun.* **2004**, *7*, 209−212.

(29) (a) Yoon, K.; Parkin, G. Artificial Manipulation of Apparent Bond Lengths as Determined by Single-Crystal X-ray Diffraction. *J. Am. Chem. Soc.* **1991**, *113*, 8414−8418. (b) Yoon, K.; Parkin, G. Resolved and Unresolved Crystallographic Disorder Between {η^3-HB(3-Bu^tpz)$_3$}ZnCN and {η^3-HB(3-Bu^tpz)$_3$}ZnX (X = Cl, Br, I). *Inorg. Chem.* **1992**, *31*, 1656−1662.

(30) (a) Adams, H.; Batten, S. R.; Davies, G. M.; Duriska, M. B.; Jeffery, J. C.; Jensen, P.; Lu, J.; Motson, G. R.; Coles, S. J.; Hursthouse, M. B.; Ward, M. D. New bis-, tris- and tetrakis-(pyrazolyl)borate ligands with 3-pyridyl and 4-pyridyl substituents: synthesis and coordination chemistry. *Dalton Trans.* **2005**, 1910−

https://dx.doi.org/10.1021/acs.inorgchem.0c02586
Inorg. Chem. 2020, 59, 17834−17850

1923. (b) Pérez Olmo, C.; Böhmerle, K.; Steinfeld, G.; Vahrenkamp, H. New Polar Pyrazolylborate Ligands and Their Basic Zinc Complex Chemistry. *Eur. J. Inorg. Chem.* **2006**, *2006*, 3869−3877. (c) Vitze, H.; Bolte, M.; Lerner, H.-W.; Wagner, M. Third-Generation Scorpionates $[RBpz_3]^-$ − How Influential Is the Nondonor Substituent R? *Eur. J. Inorg. Chem.* **2016**, *2016*, 2443−2454.

(31) (a) Shi, X.; Liu, Z.; Cheng, J. Barium tetraalkylaluminate complexes supported by the super-bulky hydrotris(pyrazolyl)borate ligand. *Dalton Trans.* **2019**, *48*, 17919−17924. (b) Shi, X.; Cheng, J. Reversible addition and hydrogenation of 1,1-diphenylethylene with a barium complex. *Dalton Trans.* **2019**, *48*, 8565−8568.

(32) Hillier, A. C.; Liu, S.-Y.; Sella, A.; Elsegood, M. R. J. Lanthanide Chalcogenolate Complexes: Synthesis and Crystal Structures of the Isoleptic Series $[Sm(Tp^{Me,Me})_2ER]$ (E = O, S, Se, Te; $Tp^{Me,Me}$ = *tris*-3,5-Dimethylpyrazolylborate). *Inorg. Chem.* **2000**, *39*, 2635−2644.

(33) Ferrence, G. M.; McDonald, R.; Morissette, M.; Takats, J. Mixed pyrazolylborate/cyclopentadienyl derivatives of divalent lanthanides: synthesis and structure of $(Tp^{tBu,Me})Yb(C_5H_4R)$ (R = H, $SiMe_3$). *J. Organomet. Chem.* **2000**, *596*, 95−101.

(34) Sun, Y.; McDonald, R.; Takats, J.; Day, V. W.; Eberspacher, T. A. Synthesis and Structure of Bis[hydrotris(3,5-dimethylpyrazolyl)-borato]iodouranium(III), $U[HB(3,5\text{-}Me_2pz)_3]_2I$: Unprecedented Side-On Interaction Involving a Hydrotris(pyrazolyl)borate Ligand. *Inorg. Chem.* **1994**, *33*, 4433−4434.

(35) (a) Qin, K.; Incarvito, C. D.; Rheingold, A. L.; Theopold, K. H. Hydrogen Atom Abstraction by a Chromium(IV) Oxo Complex Derived from O_2. *J. Am. Chem. Soc.* **2002**, *124*, 14008−14009. (b) Qin, K.; Incarvito, C. D.; Rheingold, A. L.; Theopold, K. H. A Structurally Characterized Chromium(III) Superoxide Complex Features "Side-on" Bonding. *Angew. Chem., Int. Ed.* **2002**, *41*, 2333−2335. (c) Akturk, E. S.; Yap, G. P. A.; Theopold, K. H. Mechanism-based design of labile precursors for chromium(I) chemistry. *Chem. Commun.* **2015**, *51*, 15402−15405. (d) Akturk, E. S.; Yap, G. P. A.; Theopold, K. H. Dioxygen Activation by Non-Adiabatic Oxidative Addition to a Single Metal Center. *Angew. Chem., Int. Ed.* **2015**, *54*, 14974−14977. (e) Hess, A.; Hörz, M. R.; Liable-Sands, L. M.; Lindner, D. C.; Rheingold, A. L.; Theopold, K. H. Insertion of O_2 into a Chromium−Phenyl Bond: Mechanism of Formation of the Paramagnetic d^2 Oxo Complex $[Tp^{tBu,Me}Cr^{IV}(O)\text{-}OPh]$. *Angew. Chem., Int. Ed.* **1999**, *38*, 166−168.

(36) Addison, A. W.; Rao, T. N.; Reedijk, J.; van Rijn, J.; Verschoor, G. C. Synthesis, structure, and spectroscopic properties of copper(II) compounds containing nitrogen−sulphur donor ligands; the crystal and molecular structure of aqua[1,7-bis(N-methylbenzimidazol-2′-yl)-2,6-dithiaheptane]copper(II) perchlorate. *J. Chem. Soc., Dalton Trans.* **1984**, 1349−1356.

(37) Biagini, P.; Calderazzo, F.; Marchetti, F.; Romano, A. M.; Spera, S. Synthesis and structural characterization of sterically crowded hydridotris(pyrazolyl)borato complexes: Unusual double 1,2-borotropic shift at a titanium centre. *J. Organomet. Chem.* **2006**, *691*, 4172−4180.

(38) (a) Mailer, C.; Taylor, C. P. S. Rapid adiabatic passage EPR of ferricytochrome c: Signal enhancement and determination of the spin-lattice relaxation time. *Biochim. Biophys. Acta, Protein Struct.* **1973**, *322*, 195−203. (b) Mailer, C.; Hoffman, B. M. Tumbling of an adsorbed nitroxide using rapid adiabatic passage. *J. Phys. Chem.* **1976**, *80*, 842−846.

(39) Aranzaes, J. R.; Daniel, M.-C.; Astruc, D. Metallocenes as references for the determination of redox potentials by cyclic voltammetry - Permethylated iron and cobalt sandwich complexes, inhibition by polyamine dendrimers, and the role of hydroxy-containing ferrocenes. *Can. J. Chem.* **2006**, *84*, 288−299.

(40) (a) Yang, L.; Powell, D. R.; Houser, R. P. Structural variation in copper(I) complexes with pyridylmethylamide ligands: structural analysis with a new four-coordinate geometry index, τ_4. *Dalton Trans.* **2007**, 955−964. (b) Reineke, M. H.; Sampson, M. D.; Rheingold, A. L.; Kubiak, C. P. Synthesis and Structural Studies of Nickel(0) Tetracarbene Complexes with the Introduction of a New Four-Coordinate Geometric Index, τ_δ. *Inorg. Chem.* **2015**, *54*, 3211−3217.

(41) Krzystek, J.; Zvyagin, S. A.; Ozarowski, A.; Trofimenko, S.; Telser, J. Tunable-frequency high-field electron paramagnetic resonance. *J. Magn. Reson.* **2006**, *178*, 174−183.

(42) (a) Angeli, C.; Cimiraglia, R.; Evangelisti, S.; Leininger, T.; Malrieu, J.-P. Introduction of *n*-electron valence states for multi-reference perturbation theory. *J. Chem. Phys.* **2001**, *114*, 10252−10264. (b) Angeli, C.; Cimiraglia, R.; Malrieu, J.-P. *N*-electron valence state perturbation theory: a fast implementation of the strongly contracted variant. *Chem. Phys. Lett.* **2001**, *350*, 297−305. (c) Angeli, C.; Cimiraglia, R.; Malrieu, J.-P. *n*-electron valence state perturbation theory: A spinless formulation and an efficient implementation of the strongly contracted and of the partially contracted variants. *J. Chem. Phys.* **2002**, *117*, 9138−9153.

(43) (a) Liakos, D. G.; Ganyushin, D.; Neese, F. A Multiconfigurational ab Initio Study of the Zero-Field Splitting in the Di- and Trivalent Hexaquo−Chromium Complexes. *Inorg. Chem.* **2009**, *48*, 10572−10580. (b) Sinnecker, S.; Neese, F. Spin−Spin Contributions to the Zero-Field Splitting Tensor in Organic Triplets, Carbenes and Biradicals − A Density Functional and Ab Initio Study. *J. Phys. Chem. A* **2006**, *110*, 12267−12275. (c) Duboc, C.; Ganyushin, D.; Sivalingam, K.; Collomb, M.-N.; Neese, F. Systematic Theoretical Study of the Zero-Field Splitting in Coordination Complexes of Mn(III). Density Functional Theory versus Multireference Wave Function Approaches. *J. Phys. Chem. A* **2010**, *114*, 10750−10758. (d) Neese, F. Importance of Direct Spin−Spin Coupling and Spin-Flip Excitations for the Zero-Field Splittings of Transition Metal Complexes: A Case Study. *J. Am. Chem. Soc.* **2006**, *128*, 10213−10222.

(44) (a) Lang, L.; Neese, F. Spin-dependent properties in the framework of the dynamic correlation dressed complete active space method. *J. Chem. Phys.* **2019**, *150*, 104104. (b) Maurice, R.; Bastardis, R.; Graaf, C. d.; Suaud, N.; Mallah, T.; Guihéry, N. Universal Theoretical Approach to Extract Anisotropic Spin Hamiltonians. *J. Chem. Theory Comput.* **2009**, *5*, 2977−2984.

(45) (a) Sanner, R. D.; Duggan, D. M.; McKenzie, T. C.; Marsh, R. E.; Bercaw, J. E. Structure and magnetism of μ-Dinitrogen-bis(bis(pentamethylcyclopentadienyl)titanium(II)), $\{(\eta^5\text{-}C_5(CH_3)_5)_2Ti\}_2N_2$. *J. Am. Chem. Soc.* **1976**, *98*, 8358−8365. (b) Berry, D. H.; Procopio, L. J.; Carroll, P. J. Molecular Structure of $\{Cp_2Ti(PMe_3)\}_2(\mu\text{-}N_2)$, a Titanocene Dinitrogen Complex. *Organometallics* **1988**, *7*, 570−572. (c) Duchateau, R.; Gambarotta, S.; Beydoun, N.; Bensimon, C. , Side-on versus end-on coordination of dinitrogen to titanium(II) and mixed-valence titanium(I)/titanium(II) amido complexes. *J. Am. Chem. Soc.* **1991**, *113*, 8986−8988. (d) Beydoun, N.; Duchateau, R.; Gambarotta, S. , Synthesis and characterization of a thermally robust titanium dinitrogen complex. The crystal structure of $[\{[(Me_3Si)_2N]TiCl(pyridine)_2\}_2(\mu\text{-}\eta\text{:}\eta'\text{-}N_2)]$. *J. Chem. Soc., Chem. Commun.* **1992**, 244−246. (e) Hanna, T. E.; Lobkovsky, E.; Chirik, P. J. , Dinitrogen Activation by Titanium Sandwich Complexes. *J. Am. Chem. Soc.* **2004**, *126*, 14688−14689. (f) Hanna, T. E.; Lobkovsky, E.; Chirik, P. J. , Dinitrogen Complexes of Bis(cyclopentadienyl) Titanium Derivatives: Structural Diversity Arising from Substituent Manipulation. *Organometallics* **2009**, *28*, 4079−4088.

(46) (a) Morello, L.; Yu, P.; Carmichael, C. D.; Patrick, B. O.; Fryzuk, M. D. Formation of Phosphorus−Nitrogen Bonds by Reduction of a Titanium Phosphine Complex under Molecular Nitrogen. *J. Am. Chem. Soc.* **2005**, *127*, 12796−12797. (b) Shima, T.; Hu, S.; Luo, G.; Kang, X.; Luo, Y.; Hou, Z. Dinitrogen Cleavage and Hydrogenation by a Trinuclear Titanium Polyhydride Complex. *Science* **2013**, *340*, 1549−1552. (c) Mo, Z.; Shima, T.; Hou, Z. Synthesis and Diverse Transformations of a Dinitrogen Dititanium Hydride Complex Bearing Rigid Acridane-Based PNP-Pincer Ligands. *Angew. Chem., Int. Ed.* **2020**, *59*, 8635−8644.

(47) Huber, K. P.; Herzberg, G. *Molecular Spectra and Molecular Structure—IV. Constants of Diatomic Molecules*; Van Nostrand Reinhold: New York, 1979.

(48) (a) Durig, J. R.; Griffin, M. G.; Macnamee, R. W. Raman spectra of gases. XV: Hydrazine and hydrazine-d_4. *J. Raman Spectrosc.*

https://dx.doi.org/10.1021/acs.inorgchem.0c02586
Inorg. Chem. 2020, 59, 17834−17850

1975, *3*, 133−141. (b) Craig, N. C.; Levin, I. W. Vibrational assignment and potential function for *trans*-diazene (diimide): Predictions for *cis*-diazene. *J. Chem. Phys.* **1979**, *71*, 400−407.

(49) (a) Figueroa, J. S.; Piro, N. A.; Clough, C. R.; Cummins, C. C. A Nitridoniobium(V) Reagent That Effects Acid Chloride to Organic Nitrile Conversion: Synthesis *via* Heterodinuclear (Nb/Mo) Dinitrogen Cleavage, Mechanistic Insights, and Recycling. *J. Am. Chem. Soc.* **2006**, *128*, 940−950. (b) Gdula, R. L.; Johnson, M. J. A. Highly Active Molybdenum−Alkylidyne Catalysts for Alkyne Metathesis: Synthesis from the Nitrides by Metathesis with Alkynes. *J. Am. Chem. Soc.* **2006**, *128*, 9614−9615. (c) Bailey, B. C.; Fout, A. R.; Fan, H.; Tomaszewski, J.; Huffman, J. C.; Gary, J. B.; Johnson, M. J. A.; Mindiola, D. J. Snapshots of an Alkylidyne for Nitride Triple-Bond Metathesis. *J. Am. Chem. Soc.* **2007**, *129*, 2234−2235.

(50) Using the following convention for defining the coupling constant: $J = ({}^{HS}E - {}^{BS}E)/({}^{HS}\langle S^2\rangle - {}^{BS}\langle S^2\rangle)$. (a) Yamaguchi, K.; Takahara, Y.; Fueno, T. *Ab-Initio Molecular Orbital Studies of Structure and Reactivity of Transition Metal-OXO Compounds*; Springer: Dordrecht, The Netherlands, 1986; pp 155−184. (b) Soda, T.; Kitagawa, Y.; Onishi, T.; Takano, Y.; Shigeta, Y.; Nagao, H.; Yoshioka, Y.; Yamaguchi, K. Ab initio computations of effective exchange integrals for H−H, H−He−H and Mn_2O_2 complex: comparison of broken-symmetry approaches. *Chem. Phys. Lett.* **2000**, *319*, 223−230.

(51) Kool, L. B.; Rausch, M. D.; Alt, H. G.; Herberhold, M.; Hill, A. F.; Thewalt, U.; Wolf, B. A diazoalkane complex of titanium. *J. Chem. Soc., Chem. Commun.* **1986**, 408−409.

(52) (a) Polse, J. L.; Andersen, R. A.; Bergman, R. G. Synthesis, Structure, and Reactivity Studies of an η^2-N_2-Titanium Diazoalkane Complex. Generation and Trapping of a Carbene Complex Intermediate. *J. Am. Chem. Soc.* **1996**, *118*, 8737−8738. (b) Polse, J. L.; Kaplan, A. W.; Andersen, R. A.; Bergman, R. G. Synthesis of an η^2-N_2-Titanium Diazoalkane Complex with Both Imido- and Metal Carbene-Like Reactivity Patterns. *J. Am. Chem. Soc.* **1998**, *120*, 6316−6328. (c) Hanna, T. E.; Keresztes, I.; Lobkovsky, E.; Bernskoetter, W. H.; Chirik, P. J. Synthesis of a Base-Free Titanium Imido and a Transient Alkylidene from a Titanocene Dinitrogen Complex. Studies on Ti═NR Hydrogenation, Nitrene Group Transfer, and Comparison of 1,2-Addition Rates. *Organometallics* **2004**, *23*, 3448−3458. (d) Kaplan, A. W.; Polse, J. L.; Ball, G. E.; Andersen, R. A.; Bergman, R. G. Synthesis, Structure, and Reactivity of η^2-N_2-Aryldiazoalkane Titanium Complexes: Cleavage of the N−N Bond. *J. Am. Chem. Soc.* **1998**, *120*, 11649−11662.

(53) Anandha Babu, G.; Perumal Ramasamy, R.; Ramasamy, P.; Natarajan, S. Studies on the crystal growth, crystal structure, optical and thermal properties of an organic crystal: Benzophenone hydrazone. *J. Cryst. Growth* **2009**, *311*, 3461−3465.

(54) (a) Davis, P. J.; Harris, L.; Karim, A.; Thompson, A. L.; Gilpin, M.; Moloney, M. G.; Pound, M. J.; Thompson, C. Substituted diaryldiazomethanes and diazofluorenes: structure, reactivity and stability. *Tetrahedron Lett.* **2011**, *52*, 1553−1556. (b) Nazran, A. S.; Lee, F. L.; Gabe, E. J.; Lepage, Y.; Northcott, D. J.; Park, J. M.; Griller, D. Structures of dimesitylcarbene and related compounds. *J. Phys. Chem.* **1984**, *88*, 5251−5254.

(55) (a) Armor, J. N.; Taube, H. Reduction of nitrous oxide in the presence of pentaammineaquoruthenium(II). *J. Am. Chem. Soc.* **1971**, *93*, 6476−6480. (b) Laplaza, C. E.; Odom, A. L.; Davis, W. M.; Cummins, C. C.; Protasiewicz, J. D. Cleavage of the Nitrous Oxide NN Bond by a Tris(amido)molybdenum(III) Complex. *J. Am. Chem. Soc.* **1995**, *117*, 4999−5000. (c) Cherry, J.-P. F.; Johnson, A. R.; Baraldo, L. M.; Tsai, Y.-C.; Cummins, C. C.; Kryatov, S. V.; Rybak-Akimova, E. V.; Capps, K. B.; Hoff, C. D.; Haar, C. M.; Nolan, S. P. On the Origin of Selective Nitrous Oxide N−N Bond Cleavage by Three-Coordinate Molybdenum(III) Complexes. *J. Am. Chem. Soc.* **2001**, *123*, 7271−7286. (d) Palluccio, T. D.; Rybak-Akimova, E. V.; Majumdar, S.; Cai, X.; Chui, M.; Temprado, M.; Silvia, J. S.; Cozzolino, A. F.; Tofan, D.; Velian, A.; Cummins, C. C.; Captain, B.; Hoff, C. D. Thermodynamic and Kinetic Study of Cleavage of the N−O Bond of N-Oxides by a Vanadium(III) Complex: Enhanced Oxygen Atom Transfer Reaction Rates for Adducts of Nitrous Oxide and Mesityl Nitrile Oxide. *J. Am. Chem. Soc.* **2013**, *135*, 11357−11372.

(56) (a) Pamplin, C. B.; Ma, E. S. F.; Safari, N.; Rettig, S. J.; James, B. R. The Nitrous Oxide Complex, $RuCl_2(\eta^1\text{-}N_2O)(P{-}N)(PPh_3)$ (P−N = [*o*-(*N*,*N*-Dimethylamino)phenyl]diphenylphosphine); Low Temperature Conversion of N_2O to N_2 and O_2. *J. Am. Chem. Soc.* **2001**, *123*, 8596−8597. (b) Piro, N. A.; Lichterman, M. F.; Harman, W. H.; Chang, C. J. A Structurally Characterized Nitrous Oxide Complex of Vanadium. *J. Am. Chem. Soc.* **2011**, *133*, 2108−2111. (c) Zhuravlev, V.; Malinowski, P. J. A Stable Crystalline Copper(I)−N_2O Complex Stabilized as the Salt of a Weakly Coordinating Anion. *Angew. Chem., Int. Ed.* **2018**, *57*, 11697−11700. (d) Gyton, M. R.; Leforestier, B.; Chaplin, A. B. Rhodium(I) Pincer Complexes of Nitrous Oxide. *Angew. Chem., Int. Ed.* **2019**, *58*, 15295−15298. (e) Mokhtarzadeh, C. C.; Chan, C.; Moore, C. E.; Rheingold, A. L.; Figueroa, J. S. Side-On Coordination of Nitrous Oxide to a Mononuclear Cobalt Center. *J. Am. Chem. Soc.* **2019**, *141*, 15003−15007.

(57) (a) Graham, T. W.; Kickham, J.; Courtenay, S.; Wei, P.; Stephan, D. W. Reduction of Titanium(IV)-Phosphinimide Complexes: Routes to Ti(III) Dimers, Ti(IV)-Metallacycles, and Ti(II) Species. *Organometallics* **2004**, *23*, 3309−3318. (b) Boynton, J. N.; Guo, J.-D.; Grandjean, F.; Fettinger, J. C.; Nagase, S.; Long, G. J.; Power, P. P. Synthesis and Characterization of the Titanium Bisamide $Ti\{N(H)Ar^{iPr6}\}_2$ (Ar^{iPr6} = C_6H_3-2,6-(C_6H_2-2,4,6-$^iPr_3$)$_2$ and Its $TiCl\{N(H)Ar^{iPr6}\}_2$ Precursor: Ti(II) → Ti(IV) Cyclization. *Inorg. Chem.* **2013**, *52*, 14216−14223. (c) Aguilar-Calderón, J. R.; Murillo, J.; Gomez-Torres, A.; Saucedo, C.; Jordan, A.; Metta-Magaña, A. J.; Pink, M.; Fortier, S. Redox Character and Small Molecule Reactivity of a Masked Titanium(II) Synthon. *Organometallics* **2020**, *39*, 295−311. (d) Gómez-Torres, A.; Aguilar-Calderón, J. R.; Encerrado-Manriquez, A. M.; Pink, M.; Metta-Magaña, A. J.; Lee, W.-Y.; Fortier, S. Titanium-Mediated Catalytic Hydrogenation of Monocyclic and Polycyclic Arenes. *Chem. - Eur. J.* **2020**, *26*, 2803−2807. (e) Gómez-Torres, A.; Aguilar-Calderón, J. R.; Saucedo, C.; Jordan, A.; Metta-Magaña, A.; Pinter, B.; Fortier, S. Reversible oxidative-addition and reductive-elimination of thiophene from a titanium complex and its thermally-induced hydrodesulphurization chemistry. *Chem. Commun.* **2020**, *56*, 1545−1548.

(58) (a) Carpino, L. A.; Padykula, R. E.; Barr, D. E.; Hall, F. H.; Krause, J. G.; Dufresne, R. F.; Thoman, C. J. Synthesis, Characterization, and Thermolysis of 7-Amino-7-azabenzonorbornadienes. *J. Org. Chem.* **1988**, *53*, 2565−2572. (b) Mindiola, D. J.; Cummins, C. C. Deprotonated 2,3:5,6-Dibenzo-7-aza bicyclo[2.2.1]hepta-2,5-diene as a Nitrido Nitrogen Source by Anthracene Elimination: Synthesis of an Iodide(nitride)chromium(VI) Complex. *Angew. Chem., Int. Ed.* **1998**, *37*, 945−947.

(59) (a) McKarns, P. J.; Yap, G. P. A.; Rheingold, A. L.; Winter, C. H. Synthesis, Structure, and Characterization of the Hydrogen-Substituted Imido Complex $TiCl_2(NH)(OPPh_3)_2$. *Inorg. Chem.* **1996**, *35*, 5968−5969. (b) Tran, B. L.; Washington, M. P.; Henckel, D. A.; Gao, X.; Park, H.; Pink, M.; Mindiola, D. J. A four coordinate parent imide *via* a titanium nitridyl. *Chem. Commun.* **2012**, *48*, 1529−1531. (c) Thompson, R.; Chen, C.-H.; Pink, M.; Wu, G.; Mindiola, D. J. A Nitrido Salt Reagent of Titanium. *J. Am. Chem. Soc.* **2014**, *136*, 8197−8200. (d) Grant, L. N.; Pinter, B.; Kurogi, T.; Carroll, M. E.; Wu, G.; Manor, B. C.; Carroll, P. J.; Mindiola, D. J. Molecular titanium nitrides: nucleophiles unleashed. *Chem. Sci.* **2017**, *8*, 1209−1224. (e) Grant, L. N.; Pinter, B.; Gu, J.; Mindiola, D. J. Molecular Zirconium Nitride Super Base from a Mononuclear Parent Imide. *J. Am. Chem. Soc.* **2018**, *140*, 17399−17403.

(60) (a) Cummins, C. C.; Schrock, R. R.; Davis, W. M. Synthesis of Terminal Vanadium(V) Imido, Oxo, Sulfido, Selenido, and Tellurido Complexes by Imido Group or Chalcogenide Atom Transfer to Trigonal Monopyramidal V[N_3N] (N_3N = $[(Me_3SiNCH_2CH_2)_3N]^{3-}$). *Inorg. Chem.* **1994**, *33*, 1448−1457. (b) Smythe, N. C.; Schrock, R. R.; Müller, P.; Weare, W. W. Synthesis of $[(HIPTNCH_2CH_2)_3N]V$ Compounds (HIPT = 3,5-(2,4,6-*i*-$Pr_3C_6H_2$)$_2C_6H_3$) and an Evaluation of Vanadium for the

https://dx.doi.org/10.1021/acs.inorgchem.0c02586
Inorg. Chem. 2020, 59, 17834−17850

Reduction of Dinitrogen to Ammonia. *Inorg. Chem.* **2006**, *45*, 9197−9205. (c) Hulley, E. B.; Bonanno, J. B.; Wolczanski, P. T.; Cundari, T. R.; Lobkovsky, E. B. Pnictogen-Hydride Activation by $(silox)_3Ta$ (silox = $^tBu_3SiO$); Attempts to Circumvent the Constraints of Orbital Symmetry in N_2 Activation. *Inorg. Chem.* **2010**, *49*, 8524−8544.

(61) (a) Hanna, T. E.; Lobkovsky, E.; Chirik, P. J. N−H Group Transfer and Oxidative Addition Chemistry Promoted by Isolable Bis(cyclopentadienyl)titanium Sandwich Complexes. *Eur. J. Inorg. Chem.* **2007**, *2007*, 2677−2685. (b) Veige, A. S.; Slaughter, L. M.; Lobkovsky, E. B.; Wolczanski, P. T.; Matsunaga, N.; Decker, S. A.; Cundari, T. R. Symmetry and Geometry Considerations of Atom Transfer: Deoxygenation of $(silox)_3WNO$ and R_3PO (R = Me, Ph, ^tBu) by $(silox)_3M$ (M = V, NbL (L = PMe_3, 4-Picoline), Ta; silox = $^tBu_3SiO$). *Inorg. Chem.* **2003**, *42*, 6204−6224. (c) Bowman, A. C.; Bart, S. C.; Heinemann, F. W.; Meyer, K.; Chirik, P. J. Synthesis of Bis(imino)pyridine Iron Amide and Ammonia Compounds from an N−H Transfer Agent. *Inorg. Chem.* **2009**, *48*, 5587−5589.

https://dx.doi.org/10.1021/acs.inorgchem.0c02586
Inorg. Chem. 2020, 59, 17834−17850